Coastal Engineering 68 (2012) 78–95

Contents lists available at SciVerse ScienceDirect

Coastal Engineering

journal homepage: www.elsevier.com/locate/coastaleng

Free-stream velocity descriptions under waves with skewness and asymmetry

J. Malarkey *, A.G. Davies

School of Ocean Sciences, Bangor University, Menai Bridge, Anglesey, LL59 5AB, UK

ARTICLE INFO

Article history:
Received 20 July 2011
Received in revised form 27 April 2012
Accepted 30 April 2012
Available online 16 June 2012

Keywords:
Waves
Free-stream velocity
Wave-shoaling
Skewness
Asymmetry

ABSTRACT

In shallow water, when waves shoal their orbital velocities exhibit skewness (velocity skewness) and asymmetry (acceleration skewness) in response to corresponding changes in the free surface. Near the bed, changes in the skewness and asymmetry of the time-varying velocities have important consequences for the residual velocities 'spun up' by the bottom friction and for sediment transport. In the wave boundary layer, where the largest sediment transport often occurs, there is a need to represent the free-stream velocity (the orbital velocity at the edge of the wave boundary layer) in a systematic way such that it can be mimicked in wave tunnel experiments and wave boundary layer models which usually do not represent the free surface. Since there is no readily accessible dynamical theory for shoaling waves that includes both skewness and asymmetry, it is necessary to synthesize the shoaling effect in a free-stream velocity description that is general enough to fit observed velocity time series. This paper reviews previous free-stream velocity descriptions, including the description of Abreu et al. (2010), and introduces a new description based on generalising a sawtooth wave shape. The paper quantifies all the relevant measures of skewness and asymmetry for each description. It then demonstrates that Abreu et al.'s (2010) description represents the most general one and improves upon their fitting techniques to observed free-stream velocities to further simplify it. When this description is used in conjunction with a characterisation of the velocity for irregular waves, such as that of Elfrink et al. (2006), it is possible to relate velocity skewness and asymmetry directly to the non-dimensional wave and beach parameters (wave height, surface wavelength and surf similarity parameter as a proxy for beach slope). MATLAB scripts are provided for the improved description of Abreu et al. (2010) and Elfrink et al.'s (2006) characterisation.

1. Introduction

As waves shoal on a beach, in addition to their wavelength and height changing, e.g. Tajima and Madsen (2002), their skewness (velocity skewness) and asymmetry (acceleration skewness) also change, e.g. Doering and Bowen (1995). Skewness is the relative measure of larger orbital velocities under the wave crest compared to smaller orbital velocities under the wave trough, where as asymmetry is the relative measure of larger accelerations between trough and crest compared to smaller accelerations between crest and trough. The changes in skewness and asymmetry in the free-stream velocity, at the edge of the wave bottom boundary layer, have important implications for sediment transport in shallow, wave-dominated conditions, both in terms of bedload transport as determined by the time-varying bottom stress and suspended load transport as determined by the time-varying and residual velocities.

From the predictions of shoaling waves for a Boussinesq model, Tajima and Madsen (2002) parameterised the ratios between nonlinear and equivalent linear wave characteristics, representing the free-stream velocity, in terms of deep-water properties and beach slope. However since the study was based on a Boussinesq model, by definition the effect of asymmetry was not included. Fuhrman et al. (2009) used a numerical model of a convergent/divergent channel to isolate the various effects of skewness, asymmetry, bed slope and steady streaming on the bed stress that occur under shoaling waves and compared their importance on the basis of schematic representations of the free-stream velocity.

Gonzalez-Rodriguez and Madsen (2007) represented the effect of skewness and asymmetry on bed load transport using a bed shear stress based on a time-varying friction factor and phase lead. In contrast, Nielsen (2002) represented the asymmetry effect on bedload transport using added mass concepts in the shear stress. Drake and Calantoni (2001) and Hsu and Hanes (2004) both used a schematic representation of a shoaling wave to demonstrate the different effects of skewness and asymmetry in determining the behaviour of sheet-flow in two-phase models.

Isobe and Horikawa (1982) characterised the skewness and asymmetry of the free-stream velocity for regular shoaling waves at normal incidence in terms of the beach slope, local water depth, wave height and wavelength and deep-water wave height, based on a specified functional form. Dibajnia et al. (2001) adapted their skewness and asymmetry prescriptions for irregular waves and Grasmeijer

* Corresponding author. Tel.: +44 1248 382848; fax: +44 1248 716367.
E-mail address: j.malarkey@bangor.ac.uk (J. Malarkey).

0378-3839/$ – see front matter © 2012 Elsevier B.V. All rights reserved.
doi:10.1016/j.coastaleng.2012.04.009

and Ruessink (2003) adapted their skewness prescription so that it could be determined entirely in terms of local wave quantities. All of these adapted prescriptions retained the same functional form for the free-stream velocity. More recently, based on a large amount of field data, Elfrink et al. (2006) characterised the shape of the free-stream velocity for irregular shoaling waves at normal incidence, in terms of local wave quantities based on a different functional form to that of Isobe and Horikawa (1982). However, as pointed out by Abreu et al. (2010), both the functional forms of Isobe and Horikawa (1982) and Elfrink et al. (2006) resulted in accelerations which were discontinuous and therefore not appropriate to use directly in models.

Abreu et al. (2010) presented a general free-stream velocity description, with a continuous acceleration, and demonstrated its ability to fit to the characterisations of Elfrink et al. (2006) and Isobe and Horikawa (1982) and further to represent irregular free-stream velocity data. However, Abreu et al.'s (2010) method for determining the skewness and asymmetry parameters was rather cumbersome. Ruessink et al. (2009) fitted Abreu et al.'s (2010) description to a large amount of shoaling-wave data on a wave-by-wave basis and demonstrated that asymmetry rarely occurred without skewness. Abreu et al. (2011) subsequently used both Gonzalez-Rodriguez and Madsen's (2007) and Nielsen's (2002) methods to represent the bed shear stress.

van Rijn et al. (2011) represented the free-stream velocity for shoaling waves in cross-shore sediment transport models using the approach of Grasmeijer and Ruessink (2003), neglecting changes in asymmetry, and also used another approach based on generalising a Stokes second-order description. These different representations resulted in quite distinct variations in the free-stream velocity and consequently had different effects on the cross-shore sediment transport. In general, however, van Rijn et al. (2011) found that the cross-shore sediment transport models were better at predicting erosive rather than accretive morphological events.

For a free-stream velocity description to successfully represent the shoaling effect under real waves on the one hand and prove useful as a boundary condition in a wave boundary layer model on the other, in addition to having a continuous acceleration, it should ideally (i) be able to represent as wide a range of skewness and asymmetry as possible, (ii) be straightforward to use and (iii) have skewness and asymmetry parameters that are relatively straightforward to calculate. This paper reviews the different free-stream velocity descriptions that have been used in models and wave tunnels on the basis of these three criteria. The paper then goes on to discuss different fitting strategies to measured velocities for the free-stream descriptions and in so doing revisits Elfrink et al.'s (2006) characterisation and the representation of irregular wave sequences. The paper concludes by determining the best free-stream velocity description and provides simple procedures for its calculation and fitting to data, in to the form of MATLAB scripts, that supersedes previous work. The paper is aimed at researchers who wish to characterise irregular wave data, compare different free-stream descriptions with one another or represent the shoaling wave effect on the free-stream velocity in a model systematically.

In Section 2 the various definitions of the measures of skewness and asymmetry are given, together with an illustrative example of wave shoaling based on Elfrink et al.'s (2006) characterisation. In Section 3 the various free-stream velocity descriptions are introduced; in some cases these descriptions are generalised and in all cases their limitations are discussed. This section also presents potential fitting strategies to represent the free-stream velocity and compares the resulting descriptions' relative behaviour on theoretical grounds. In Section 4 the ability of different free-stream descriptions to fit to Elfrink et al.'s (2006) characterisation and other shoaling wave data is compared. Finally, in Sections 5 and 6 the discussion and conclusions of the study are presented.

2. Skewness, asymmetry and wave shoaling

2.1. Definitions of skewness and asymmetry

The free-stream velocity is defined as the time-varying velocity immediately outside the wave bottom boundary layer driven by the time-varying free surface of the wave. As waves shoal, the changing wave height and steepening of the surface slope on the forward side of the wave is mirrored by changes in the free-stream velocity such that changes in both skewness and asymmetry can result. Skewness (velocity skewness) and asymmetry (acceleration skewness) beneath these waves can be represented in various ways. Silva et al. (2011) defined skewness and asymmetry, in terms of extreme values in the wave cycle, by R and β as follows

$$R=\frac{u^*_{\max}}{u^*_{\max}-u^*_{\min}},\quad \beta=\frac{a^*_{\max}}{a^*_{\max}-a^*_{\min}}, \tag{1a,b}$$

where the u^* is the dimensional free-steam velocity, a^* the dimensional free-stream acceleration ($=\mathrm{d}u^*/\mathrm{d}t^*$) and the max and min subscripts correspond to maximum and minimum values in the wave cycle (all dimensional quantities are starred). Here $u^*_{\max}$ and $u^*_{\min}$ correspond to the peak velocity under the wave crest and trough and $a^*_{\max}$ and $a^*_{\min}$ correspond to peak acceleration and deceleration around the wave crest (see Fig. 1). For each parameter a value of ½ corresponds to no skewness/asymmetry. In anticipation of what is to follow, it is assumed that $u^*=U^*_1u(t)$ and $a^*=A^*_1a(t)$ where u, a and t are the non-dimensional velocity, acceleration and time ($0\le t\le 2\pi$), $U^*_1=(u^*_{\max}-u^*_{\min})/2$, $A^*_1=2\pi U^*_1/T^*$ and T^* is the wave period. With this non-dimensionalisation, $u_{\max}-u_{\min}=2$ and therefore R and β are:

$$R=\frac{u_{max}}{2},\quad \beta=\frac{a_{\max}}{a_{\max}-a_{\min}}. \tag{2a,b}$$

Alternative measures of the skewness and asymmetry adopted by Drake and Calantoni (2001), which are based on mean quantities and are dimensional, are u^*_{spike} and a^*_{spike}

$$\frac{u^*_{\mathrm{spike}}}{U^*_1}=\frac{\langle u^3\rangle}{\langle u^2\rangle},\quad \frac{a^*_{\mathrm{spike}}}{A^*_1}=\frac{\langle a^3\rangle}{\langle a^2\rangle}, \tag{3a,b}$$

where the angled brackets indicate a cycle average, and a value of 0 for each parameter corresponds to no skewness/asymmetry (it has been assumed here that $\langle u\rangle=\langle a\rangle=0$). Other researchers (see for example Hoefel and Elgar, 2003; Ruessink et al., 2009) have quantified the dimensionless skewness, S, and asymmetry, A_a or A, in terms of mean quantities by

$$S=\frac{\langle u^3\rangle}{u^3_{\mathrm{rms}}},\quad A=\frac{\langle \tilde{u}^3\rangle}{u^3_{\mathrm{rms}}},\quad A_a=\frac{\langle a^3\rangle}{a^3_{\mathrm{rms}}}, \tag{4a,b,c}$$

where $u_{\mathrm{rms}}=\langle u^2\rangle^{1/2}$, $a_{\mathrm{rms}}=\langle a^2\rangle^{1/2}$ and $\tilde{u}$ is the Hilbert transform of u (e.g. if $u=\sin t$, $\tilde{u}=-\cos t$). Quantifying the skewness and asymmetry in terms of Eqs. (3a,b) or (4a,b,c) also allows irregular wave sequences to be characterised statistically. In some cases since calculating a can be problematic an alternative to β, a^*_{spike}, A and A_a is simply

$$\alpha=\frac{t_{\max}}{\pi}, \tag{5}$$

where $t_{\max}$ is the time from zero up-crossing of the velocity to $u_{\max}$ in radians (see for example Abreu et al., 2010), such that a sinusoidal wave with no asymmetry corresponds to $\alpha=1/2$. In the literature, different measures of skewness and asymmetry are used in different contexts. For instance, irregular wave, free-stream velocities tend to be characterised by statistical measures, such as S and A, (see,

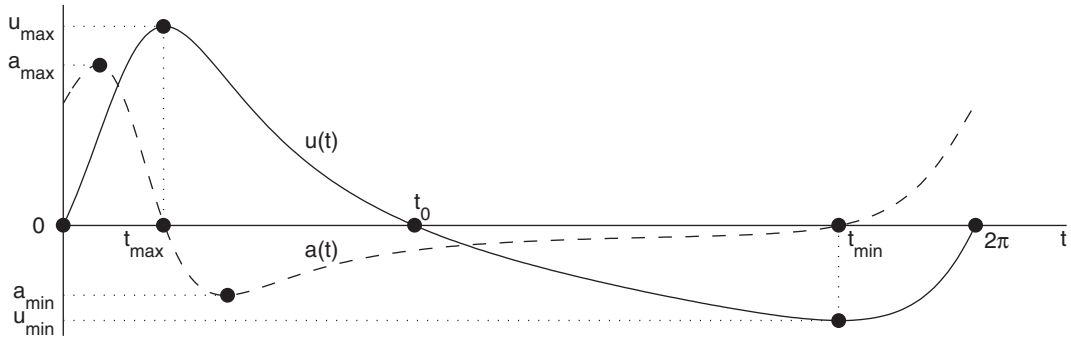

Fig. 1. Definition sketch of the non-dimensional free-stream velocity u and acceleration a time series beneath asymmetric skewed waves.

Doering and Bowen, 1995), whereas sediment transport can be characterised by either statistical, u^*_{spike} and a^*_{spike}, or extreme, R and β, measures (Drake and Calantoni, 2001; van der A et al., 2010). Since there is no consensus on how best to quantify the skewness and asymmetry, all of these different measures, Eqs. (2a,b)–(5), will be determined for each of the free-stream velocity descriptions that follow, for completeness and also because this has not been done anywhere else. However in the paper, attention will focus on R, β and α.

2.2. Elfrink et al.'s (2006) characterisation

Elfrink et al. (2006) considered a large amount of irregular shoaling wave data from three field sites on a wave-by-wave basis. By projecting the long- and cross-shore components of velocity onto the wave direction, Elfrink et al. (2006) characterised the shape of the free-stream velocity for shore-normal waves up to the breaking point using

$$u^*(t) = U_1^* \times \begin{cases} 2R\sin\left[\dfrac{\pi t}{2t_{max}}\right], & 0 < t \le t_{max}, \\ 2R\cos\left[\dfrac{\pi(t-t_{max})}{2(t_0-t_{max})}\right] - u_{01}, & t_{max} < t \le t_0, \\ -2(1-R)\sin\left[\dfrac{\pi(t-t_0)}{2(t_{min}-t_0)}\right], & t_0 < t \le t_{min}, \\ -2(1-R)\cos\left[\dfrac{\pi(t-t_{min})}{2(2\pi-t_{min})}\right], & t_{min} < t \le 2\pi, \end{cases} \quad (6)$$

where $u_{01} = U_0\sin[\pi(t-t_{max})/(t_0-t_{max})]$, t_{max}, t_0 and t_{min} are as defined in Fig. 1 and U_0 is an additional correction term. Elfrink et al. (2006) parameterised U_1^*/U_{Airy}^*, R, t_{max}, t_{min}, t_0 and U_0, where $U_{Airy}^* = \pi H^*/T^*\sinh k^*h^*$ and $k^* = 2\pi/L^*$, in terms three non-dimensional numbers: the relative wave height, normalised surface wave length and surf similarity parameter:

$$H = \frac{H^*}{h^*}, \quad L = \frac{L^*}{h^*}, \quad \xi = \frac{\tan\theta}{\sqrt{H^*/L_0^*}}, \quad (7a, b, c)$$

where h^* and H^* and are the local water depth and wave height and L^* is the wavelength from linear theory ($L^* = L_0^*\tanh k^*h^*$), L_0^* is the deep-water wavelength ($L_0^* = g^*T^{*2}/2\pi$) and tanθ is the beach slope. Since h^* was determined by the mean water depth for a measurement burst it must include a wave set-down effect (see Longuet-Higgins and Stewart, 1962). The range of applicability of Eq. (6) can be defined by $0 \le H \le 0.6$, $0 \le L \le 26$, and $-0.7 \le \xi \le 0.9$ where $0 \le |\tan\theta| \le 1/15$ and $2s \le T^* \le 14s$. In the deep-water limit u tends to the free-stream velocity determined from linear theory (namely $u = \sin t$, $U_1^* = U_{Airy}^*$). Appendix A reposes Elfrink et al.'s (2006) parameterisation for U_1^*/U_{Airy}^*, R, t_{max}, t_{min}, t_0 and U_0 entirely in terms of non-dimensional quantities rather than in the dimensional quantities given in the original paper.

With Elfrink et al.'s (2006) characterisation it is possible to demonstrate how the free-stream velocity changes as shore-normal waves shoal over a beach of constant slope prior to wave breaking provided that H and L (H^*/h^* and L^*/h^*) can be determined. The simplest way to determine H^* and L^* is through the conservation of energy flux ($L^*H^{*2}[1 + 2k^*h^*/\sinh 2k^*h^*] = L_0^*H_0^{*2}$, where H_0^* is the deep-water wave height). Based on Boussinesq model results, Tajima and Madsen (2002) provided a parameterisation to modify H^* such that it includes non-linear wave effects. However in the case considered here, this was found to have a negligible effect on the results. In Fig. 2 the case of a 5 s wave with a deep-water wave height, H_0^*, of 0.95 m is allowed to shoal over a beach slope of 1/40 with water depths ranging from 10 to 2 m without breaking and H^* determined by the conservation of energy flux. The effect of wave set-down on the water depth, h^*, is not included, but was found to result in a less than 1% difference in U_{Airy}^* and a less than 0.2% difference R, for the case considered here. It is apparent that the wave amplitude, U_1^*, increases as the wave shoals as a result of the wave height increasing and wavelength decreasing. It is also clear from this figure that both the skewness, R, and asymmetry, β, change simultaneously as the waves shoal and that they are always greater than ½ (the crest velocity is greater than the trough velocity, $u_{max} > |u_{min}|$ and $a_{max} > |a_{min}|$). Finally it can be seen, as pointed out by Abreu et al. (2010), that the acceleration is discontinuous. The discontinuous nature of the acceleration together with the fact that Eq. (6) does not intrinsically have a zero mean without some constraints placed on R, t_{max}, t_{min}, t_0 and U_0, see Appendix A, are the main reason for seeking a more suitable functional form for the velocity. This free-stream velocity description should be general enough so that it is able to fit to Elfrink et al.'s (2006) characterisation, or indeed other characterisations such as that of Isobe and Horikawa (1982), and also represent irregular wave data in a systematic way.

It can be anticipated that the fitting of a free-stream velocity description to an observed velocity time series, between two consecutive zero up-crossings (see Fig. 1) is carried out on the basis of matching the skewness and asymmetry parameters or the relative phases and sizes of the maxima and/or minima of velocity. Also in the next section it is assumed that the free-stream velocities and associated accelerations have been non-dimensionalised by U_1^* and A_1^*.

3. Free-stream velocity descriptions

3.1. Generalised Stokes Second Order free-stream velocity

In oscillating flow tunnels, see for example Ribberink and Al-Salem (1995) and O'Donoghue et al. (2006), the non-dimensional, free-stream velocity and acceleration for a Stokes second-order

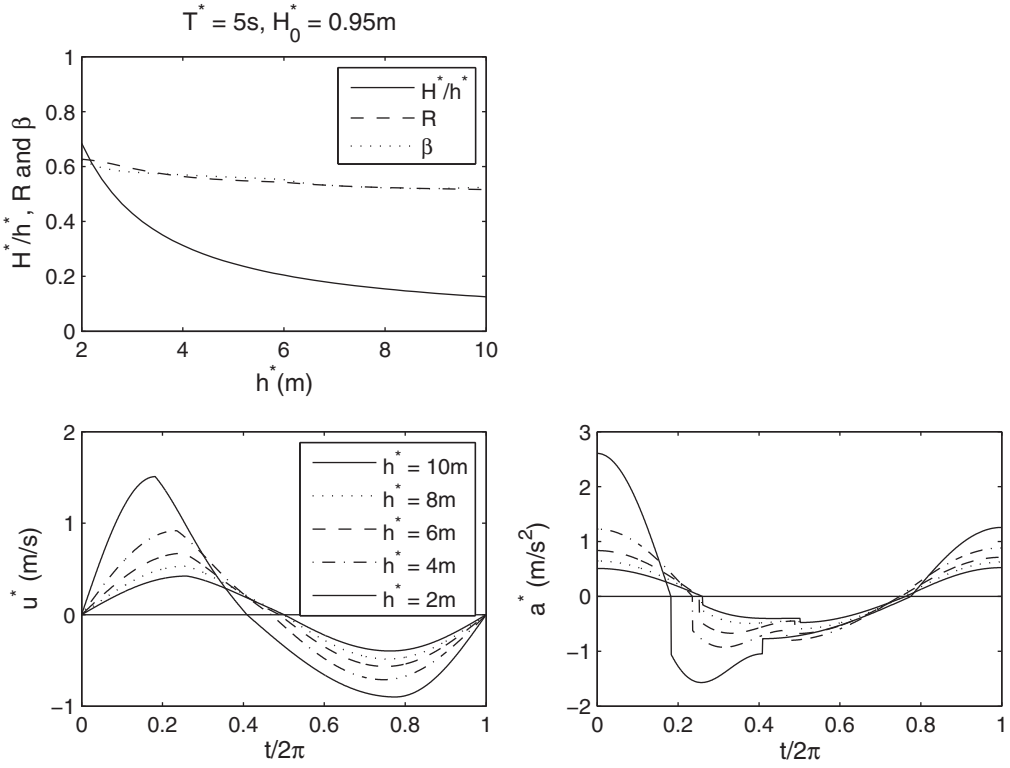

Fig. 2. Non-dimensional wave height, skewness and asymmetry and time series of the dimensional velocity and acceleration at selected heights for shoaling waves with a period of 5 s over a beach slope of 1/40 using the characterisation of Elfrink et al. (2006).

wave can be simulated as a horizontally uniform motion (because there are no vertical velocity effects) using

$$u(t) = \sin t - b\cos 2t, \quad a(t) = \cos t + 2b\sin 2t, \tag{8a, b}$$

where $0 \le t \le 2\pi$. Here b is usually restricted to the range $0 \le b \le ¼$. The velocity and acceleration for the case of $b = ¼$ is shown in Fig. 3 (curve marked $\varphi = \pi/2$). Here the peak crest velocity ($u_{max} = 1 + b$) at $t = \pi/2$ is larger in magnitude than the peak trough velocity ($u_{min} = b - 1$) at $t = 3\pi/2$ and $u_{max} - u_{min} = 2$. However, the acceleration is symmetric

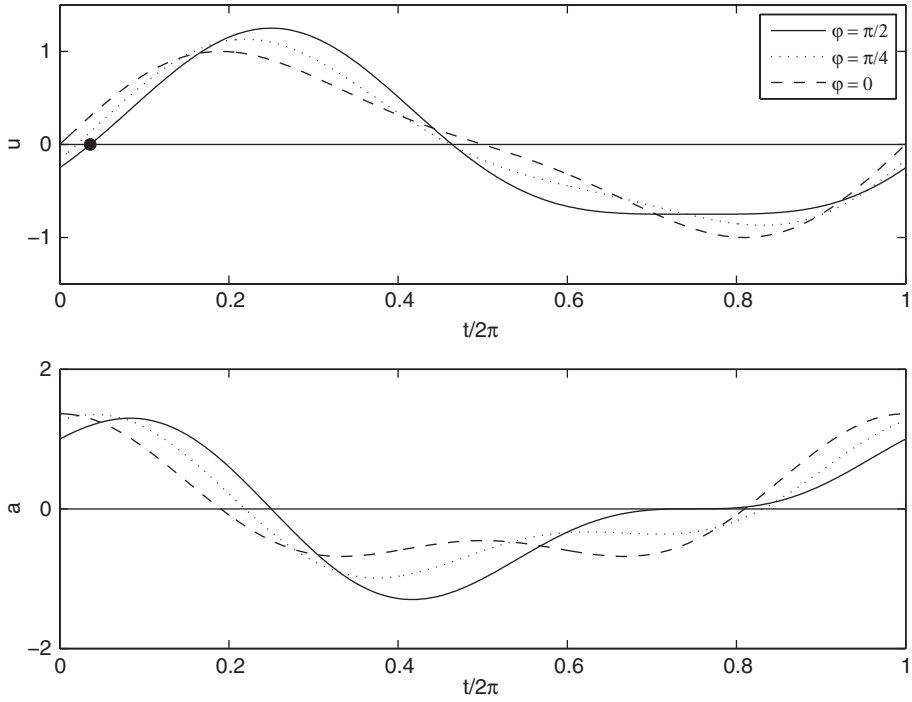

Fig. 3. Free-stream velocity and acceleration for the GSSO description, as defined by Eqs. (10a,b) with $b = ¼$, for selected φ. Dot marks the zero up-crossing, $t = \gamma$, for $\varphi = \pi/2$.

about u_{max} and u_{min} so that $a_{min} = -a_{max}$. These facts, together with the zero up-crossing phase, allow R, β and α to be expressed as

$$R = \frac{1}{2}(1+b), \quad \beta = \frac{1}{2}, \quad \alpha = \frac{1}{2} - \frac{\gamma}{\pi}, \tag{9a, b, c}$$

where γ is the zero up-crossing phase (see Fig. 3) given by $\arcsin\{[(1+8b^2)^{1/2}-1]/4b\}$. From Eq. (9a) it can be seen that since $0 \le b \le 1/4$ this means that $1/2 \le R \le 5/8$. When $b > 1/4$ an unphysical secondary maximum appears in the wave trough at $t = 3\pi/2$. The peak is unphysical because it is not observed in real waves and reflects the fact that a higher-order Stokes theory is required, since Stokes second-order waves require that $b \ll 1$.

Fuhrman et al. (2009) and van Rijn et al. (2011) generalised Eq. (8a,b) by including a waveform parameter, φ (see Elgar and Guza, 1985), which allows wave shoaling to be represented in a schematic way

$$u(t) = f(b,\varphi)[\sin t + b\sin(2t-\varphi)], \tag{10a}$$

$$a(t) = f(b,\varphi)[\cos t + 2b\cos(2t-\varphi)], \tag{10b}$$

where $f(b,\varphi)$ ensures normalisation ($u_{max} - u_{min} = 2$) and $\varphi = \pi/2$ corresponds to skewness only (a Stokes 2nd Order wave) and $\varphi = 0$ corresponds to asymmetry only (a sawtooth wave). Time series of u and a from Eqs. (10a,b), hereafter referred to as the Generalised Stokes Second Order (GSSO) description, with $b = 1/4$ and $\varphi = \pi/2$, $\pi/4$ and 0 are shown in Fig. 3. As waves shoal it can be anticipated that b will increase and φ will decrease in order to represent the behaviour shown in Fig. 2. It is important to notice also in Fig. 3 that even though there is no secondary maximum in the velocity, because $b = 1/4$, there is one in the acceleration (in the sawtooth case). For a given φ, the maximum value of b (b_{max}) such that there is no secondary maximum in u can be expressed as $\varphi = 2\arccos(X) - \arccos(X/2b_{max})$, for $0 \le \varphi \le \pi/2$, where $X = [(16b_{max}^2 - 1)/3]^{1/2}$, which results in b_{max} being in the range $1/4 \le b_{max} \le 1/2$.

3.1.1. GSSO skewness and asymmetry and fitting

In Eqs. (10a,b) when $\varphi = \pi/2$, $f = 1$ and R, β and α are given by Eq. (9a,b,c) and when $\varphi = 0$ and $R = 1/2$, based on the conditions required for $a = 0$ and $da/dt = 0$, f, α and β can be expressed as

$$f(b,0) = \frac{1}{\sin t_{max} + b\sin 2t_{max}}, \quad \alpha(b,0) = \frac{t_{max}}{\pi}, \tag{11a, b}$$

$$\beta(b,0) = \begin{cases} \dfrac{1}{2} + b, & b \le \dfrac{1}{8}, \\ \dfrac{32b^2 + 16b}{64b^2 + 16b + 1}, & b > \dfrac{1}{8}, \end{cases} \tag{11c}$$

where $t_{max} = \arccos\{[(1+32b^2)^{1/2} - 1]/8b\}$. Thus for $\varphi = 0$ and $\pi/2$, it can be seen that Eqs. (10a,b) can be fitted to an observed free-stream velocity simply by determining b, either by matching to the observed t_{max} or β for $\varphi = 0$ or the observed R for $\varphi = \pi/2$. However, the general expressions for $f(b,\varphi)$, R, β and α are quite cumbersome because they involve the solution to quartic equations (see Appendix B), which arises because of the possibility of the secondary maxima in u and a. Expressions for u^*_{spike}, a^*_{spike}, S, A_a and A are determined in Appendix C and listed in Table 1. Notice in Table 1 that $A = -S\tan\varphi$, which will be the case for all the descriptions presented in this section.

3.1.2. Fitting the GSSO description to observed velocities

Because the general expressions for $f(b,\varphi)$, R, β and α are cumbersome to determine, this means that fitting the GSSO description to an observed free-stream velocity on a wave-by-wave basis is likewise cumbersome. To some extent van Rijn et al. (2011) circumvented this problem by treating it dimensionally ($U_1^* f$ is one quantity) and characterising the wave velocities in terms of the statistical quantities S, A and u^*_{rms}. Thus since $A = -S\tan\varphi$, it followed that $\varphi = \arctan(-A/S)$ and b was determined by the GSSO expressions for S and u^*_{rms}. However, a solution to a quartic is still required to determine R, β and α exactly.

3.2. Free-stream velocity of Drake and Calantoni (2001) and Abreu et al. (2010)

The GSSO description given by Eqs. (10a,b) can be generalised still further to include higher harmonics, by analogy with Stokes higher-order theories, so that the constraint on b no longer applies. Then the normalised free-stream velocity and acceleration, are given by

$$u(t) = f(b,\varphi)\sum_{n=1}^{N} b^{n-1}\sin[nt + (1-n)\varphi], \tag{12a}$$

$$a(t) = f(b,\varphi)\sum_{n=1}^{N} nb^{n-1}\cos[nt + (1-n)\varphi], \tag{12b}$$

where again φ is the waveform parameter and $f(b,\varphi)$ ensures normalisation, $u_{max} - u_{min} = 2$, so a Stokes-type wave can be represented by $\varphi = \pi/2$ and a sawtooth wave by $\varphi = 0$ and with $N = 2$, Eqs. (12a), (12b) revert back to Eqs. (10a,b). Drake and Calantoni (2001) and Hsu and Hanes (2004) used Eqs. (12a,b) to prescribe the free-stream flow in oscillatory sheet-flow models with $b = 1/2$, $N = 5$ and $\varphi = 0$, $\pi/4$, $\pi/2$. More recently, Eqs. (12a,b) were used to represent sawtooth waves, with $b = 1/2$ and $\varphi = 0$, in a model of a constricting tunnel with $N = 16$ (Fuhrman et al., 2009) and in an experiment consisting of two concentric cylinders with $N = 20$ (Galan et al., 2011). The use of a higher number of harmonics in these latter cases made the signal smoother.

Table 1
Expressions for u^*_{spike}, a^*_{spike}, S, A_a and A, for the various free stream velocity descriptions. The procedure for calculating the normalisation f in the expressions for Eqs. (10a,b) is given in Appendix B.

Description equation	u^*_{spike}/U_1^*	a^*_{spike}/A_1^*	S	A	A_a
Stokes (8a,b)	$\frac{3b}{2(1+b^2)}$	0	$\frac{3b}{\sqrt{2(1+b^2)^3}}$	0	0
GSSO (10a,b)	$\frac{3bf\sin\varphi}{2(1+b^2)}$	$\frac{3bf\cos\varphi}{1+4b^2}$	$\frac{3b\sin\varphi}{\sqrt{2(1+b^2)^3}}$	$-\frac{3b\cos\varphi}{\sqrt{2(1+b^2)^3}}$	$\frac{3\sqrt{2}b\cos\varphi}{(1+4b^2)^{3/2}}$
ABR (16a,b)	$\frac{3}{2}b\sin\varphi$	$\frac{3b\cos\varphi}{1-b^2}$	$\frac{3b\sin\varphi}{\sqrt{2(1-b^2)}}$	$-\frac{3b\cos\varphi}{\sqrt{2(1-b^2)}}$	$\frac{3\sqrt{2}b\cos\varphi}{\sqrt{1-b^4}}$
ABR (20)	$\frac{3}{2}c$	$\frac{3b_1\sqrt{1-c^2/b_1^2}}{1-b_1^2}$	$\frac{3c}{\sqrt{2(1-b_1^2)}}$	$-3b_1\sqrt{\frac{1-c^2/b_1^2}{2(1-b_1^2)}}$	$3b_1\sqrt{\frac{2(1-c^2/b_1^2)}{1-b_1^4}}$
GSAW (26a,b)	$\frac{6P_1X(b)\sin\varphi_a}{\mathrm{Li}_2(b^2)}$	$\frac{3P_1b^2\cos\varphi}{1-b^2}$	$\frac{3\sqrt{2}X(b)\sin\varphi_a}{\mathrm{Li}_2^{1.5}(b^2)}$	$-\frac{3\sqrt{2}X(b)\cos\varphi_a}{\mathrm{Li}_2^{1.5}(b^2)}$	$\frac{3b\cos\varphi}{\sqrt{2(1-b^2)}}$

[a] Li_2 and $X(b)$ are given by Eq. (D3a,b).

Abreu et al. (2010) demonstrated that in the limit of $N=\infty$ Eqs. (12a,b) could be expressed

$$u(t) = f(r,\varphi)\frac{\sin t - Q}{1 - r\cos(t-\varphi)}, \tag{13a}$$

$$a(t) = f(r,\varphi)\frac{\cos t - r\cos\varphi + Qr\sin(t-\varphi)}{[1 - r\cos(t-\varphi)]^2}, \tag{13b}$$

where $r = 2b/(1+b^2)$, $Q = r\sin\varphi/(1+P)$, $P = (1-r^2)^{1/2}$ and $f(r,\varphi) = P$ ensures normalisation (here φ is opposite in sign to the convention in Abreu et al., 2010). This description, hereafter referred to as the ABR description, was used as the wave driver in the TRANSKEW experiments (see Silva et al., 2011) for periods of 7 and 10 s and maximum velocities up to 1.5 m/s. These experiments were undertaken to examine the relative importance of skewness and asymmetry in sediment transport. Comparisons between the ABR and Drake and Calantoni descriptions are given by Abreu et al. (2010). As with Eqs. (12a,b), a Stokes-type wave corresponds to $\varphi = \pi/2$ and a sawtooth-type wave to $\varphi = 0$. Time series of u and a from Eqs. (13a,b) with $b = ½$ for $\varphi = \pi/2$, $\pi/4$, and 0 (the settings used by Drake and Calantoni, 2001) are shown in Fig. 4. It can be seen that because a larger b is permissible these time series are more extreme in terms of skewness and asymmetry than those depicted in Fig. 3 (for $\varphi = \pi/2$, $R = ¾$ compared with ⅝ and, for $\varphi = 0$, $\beta = 0.852$ compared with ⅔).

3.2.1. ABR skewness and asymmetry

Abreu et al. (2010) showed that for a Stokes-type wave ($\varphi = \pi/2$), R and β could be expressed as

$$R(r,\pi/2) = \frac{1+r+P}{2(1+P)}, \quad \beta(r,\pi/2) = \frac{1}{2}, \tag{14a, b}$$

and for a sawtooth-type wave ($\varphi = 0$), R, β and α could be expressed as

$$R(r,0) = \frac{1}{2}, \quad \beta(r,0) = \begin{cases} \dfrac{1+r}{2}, & 0 \le r < \dfrac{1}{2}, \\ \dfrac{4r(1+r)}{4r(1+r)+1}, & \dfrac{1}{2} \le r < 1, \end{cases} \tag{15a, b}$$

$$\alpha(r,0) = \frac{1}{\pi}\arccos(r). \tag{15c}$$

However, Abreu et al.'s (2010) general parameterisations of R, β and α for the ABR description were quite cumbersome, since they required a cubic equation to be solved, were approximate and had no explicit dependence on φ; these parameterisations are improved upon below.

The velocity and acceleration for the ABR description, Eqs. (13a,b), can be expressed in terms of b rather than r, such that they are consistent with Eqs. (10a,b) and (12a,b)

$$u(t) = f(b,\varphi)\frac{\sin t - b\sin\varphi}{1 + b^2 - 2b\cos(t-\varphi)}, \tag{16a}$$

$$a(t) = f(b,\varphi)\frac{(1+b^2)\cos t - 2b\cos\varphi + 2b^2\sin\varphi\sin(t-\varphi)}{\left[1 + b^2 - 2b\cos(t-\varphi)\right]^2}, \tag{16b}$$

where $b = r/(1+P)$ ($0 \le b < 1$, $-\pi < \varphi \le \pi$). With this form for the ABR description, Appendix E demonstrates that by considering the positions of the maxima and minima it is possible to show that $f(b,\varphi) = 1 - b^2$, independent of φ, equivalent to $f(r,\varphi) = P$, and also that R is given exactly by

$$R = \frac{1}{2}(1 + b\sin\varphi). \tag{17}$$

This is consistent with Abreu et al.'s (2010) expressions for $R(r,0)$ and $R(r,\pi/2)$, Eqs. (14a) and (15a), and is considerably simpler than their

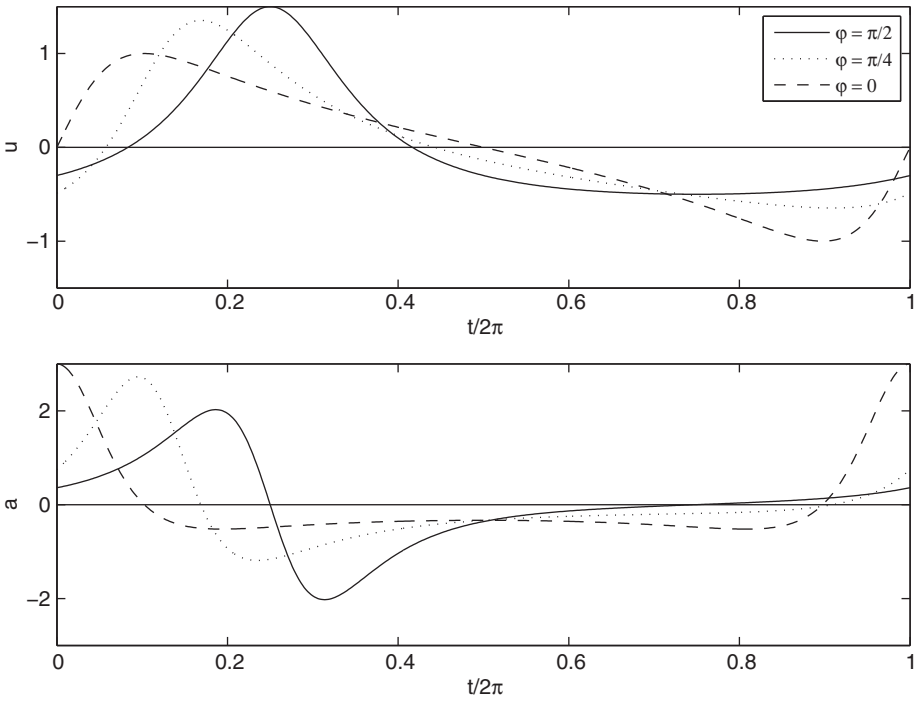

Fig. 4. Free-stream velocity and acceleration for the ABR description, as defined by Eqs. (13a,b) with $b = ½$ ($r = 0.8$), for selected φ.

approximate cubic equation solution. As with the GSSO description (see Section 3.1), the exact general expression for β in the ABR description requires the solution of a quartic equation (see Appendix B), which is cumbersome. However, based on fitting to this exact value of β, using the two special known cases of $\beta(r,\pi/2)$ and $\beta(r,0)$, Eqs. (14b) and (15b), and the fact that $\beta(r,\pi)=1-\beta(r,0)$, the following approximate parameterisation was developed

$$\beta=\frac{1}{2}+\left[\beta(r,0)-\frac{1}{2}\right]\frac{\sin\left[\left(\frac{1}{2}\pi-|\varphi|\right)F_0(r)\right]}{\sin\left[\frac{1}{2}\pi F_0(r)\right]}, \tag{18}$$

where $F_0(r)$ is given by

$$F_0(r)=\begin{cases}1-0.27(2r)^{2.1}, & r\le 0.5,\\ 0.59+0.14(2r)^{-6.2}, & r>0.5.\end{cases}$$

This parameterisation is accurate to within 0.6% of the true value and has explicit dependence upon φ. Making use of the expression for the time of the maximum in the velocity (Appendix E) and noticing from Eq. (16a) that the zero up-crossing ($t=\gamma$) is given by $\gamma=\arcsin(b\sin\varphi)$, the following general expression for α can be derived

$$\alpha=\frac{1}{\pi}\times\begin{cases}\alpha_1-\gamma, & |\varphi|\le\frac{1}{2}\pi,\\ \pi-\alpha_1-\gamma, & |\varphi|>\frac{1}{2}\pi,\end{cases} \tag{19}$$

where $\gamma=\arcsin(c)$, $c=b\sin\varphi=2R-1$ and α_1 is given by

$$\alpha_1=\arcsin\left[\frac{4c\left(b^2-c^2\right)+\left(1-b^2\right)\left(1+b^2-2c^2\right)}{\left(1+b^2\right)^2-4c^2}\right].$$

It can be seen from Eq. (19) that when $\varphi=0$, since $\sin\alpha_1=(1-b^2)/(1+b^2)=P$, then it follows that $\alpha(b,0)=\pi^{-1}\arcsin(P)$ which is equivalent to Abreu et al.'s (2010) expression for $\alpha(r,0)$, see Eq. (15c), and when $\varphi=\pi/2$, it follows that $\alpha=\pi^{-1}\arccos(b)$. Again Eq. (19) is exact so it represents an improvement upon Abreu et al.'s (2010) approximate parameterisation. Expressions for u^*_{spike}, a^*_{spike}, S, A_a and A are determined in Appendix C using the velocity and acceleration as defined by Eqs. (12a,b) in the limit of $N\to\infty$. These expressions are listed in Table 1. Since $f(b,\varphi)=1-b^2$, it can be seen that u^*_{spike}, a^*_{spike}, S, A_a and A from the ABR description are the same as those from the GSSO description, Eqs. (10a,b), to order b, as would be expected. For Eqs. (12a,b), when N is finite, u^*_{spike}, a^*_{spike}, S, A_a and A can still be determined, see Appendix C, however they will all involve sums from 1 to N. Also determining exact expressions for f, R, β and α involves the solution of equations with higher orders than the quartic involved in the GSSO description.

3.2.2. Fitting the ABR description to observed velocities

With the substitution of $c=2R-1=b\sin\varphi$ and $b_1(1-c^2/b_1^2)^{1/2}=b\cos\varphi$, such that $|b_1|=b$, Eq. (16a) can be expressed in terms of R and b_1

$$u(t)=\left(1-b_1^2\right)\frac{\sin t_1-c}{1+b_1^2-2b_1\sqrt{1-c^2/b_1^2}\cos t_1-2c\sin t_1}, \tag{20}$$

where $t_1=t+\gamma$, $\gamma=\arcsin(c)$, which ensures that $u(0,2\pi)=0$, and $|b_1|\ge|c|$. In comparing Eq. (20) with Eq. (16a), it can be seen that, when $\varphi<0$, then $c<0$ and, when $|\varphi|>\pi/2$, then $b_1<0$. Thus Eq. (20) represents a family of velocity descriptions determined by the value of b_1, but all with skewness R. Thus to fit Eq. (20) to a particular wave shape, of skewness R, between two consecutive zero up-crossings it is only necessary to determine b_1. With the substitution $c=b\sin\varphi$ and $b_1(1-c^2/b_1^2)^{1/2}=b\cos\varphi$, the expressions for u^*_{spike}, a^*_{spike}, S, A_a and A can also be expressed simply in terms of R and b_1, see Table 1. So in principle b_1 can be determined from a^*_{spike}, S, A_a, A or β, from Eq. (18), for the particular wave shape (notice that u^*_{spike} is only dependant on R). The parameter b_1 can also be determined by least-squares-fitting. However, the most direct way to determine b_1 is by matching the positions of the maximum and/or minimum in the velocity, as demonstrated by Abreu et al. (2010). From Eq. (E2), the maximum/minimum in the velocity can be expressed as a quadratic in b_1^2

$$b_1^4-2B_1b_1^2+B_2=0, \tag{21}$$

where $B_1=2\sec^2t_{1n}(1+c^2-2c\sin t_{1n})-1$ and $B_2=1+4c^2\sec^2t_{1n}(c-\sin t_{1n})^2$ and $t_{1n}=t_{\max}+\gamma$ or $t_{\min}+\gamma$, so that b_1 is given by

$$b_1=\pm\sqrt{B_1\pm\sqrt{B_1^2-B_2}}. \tag{22}$$

Here, only the negative root inside the square root sign is physically significant, but b_1 can be positive or negative depending on whether t_{1n} is greater than or less than π/2 for $t_{\max}$ or 3π/2 for $t_{\min}$. In the special case of an asymmetric, unskewed wave $R=½$ ($c=0$), $\gamma=0$, $t_{1n}=t_{\max}$ or $t_{\min}$ and $t_{\min}=2\pi-t_{\max}$. Therefore $B_2=1$, $B_1=2\sec^2t_{1n}-1=\sec^2t_{1n}+\tan^2t_{1n}$ $(B_1^2-B_2)^{1/2}=2|\sec t_{1n}||\tan t_{1n}|$ and $b_1=\pm(\sec t_{\max}-\tan t_{\max})$ if $t_{\max}<\pi/2$ or $t_{\max}>\pi/2$. In the special case of a symmetric, skewed wave, with $|b_1|=|c|$ and $t_{1n}=\pi/2$ or 3π/2, Eq. (22) can no longer be used and instead $b_1=|c|$. Thus Eq. (22) can be generalised to:

$$b_1=\begin{cases}\sqrt{B_1-\sqrt{B_1^2-B_2}}, & t_{1n}<\frac{1}{2}\pi \text{ or } t_{1n}>\frac{3}{2}\pi,\\ |c|, & t_{1n}=\frac{1}{2}\pi \text{ or } t_{1n}=\frac{3}{2}\pi,\\ -\sqrt{B_1-\sqrt{B_1^2-B_2}}, & t_{1n}>\frac{1}{2}\pi \text{ or } t_{1n}<\frac{3}{2}\pi,\end{cases} \tag{23}$$

where $t_{1n}=t_{\max}+\gamma$ or $t_{\min}+\gamma$. In the general case, for an asymmetric, skewed wave, the phases of $t_{\max}$ and $t_{\min}$ cannot both be satisfied by a single value of b_1. The choice of which value of b_1 to use under these circumstances is discussed later. Unlike Abreu et al.'s (2010) approximate fitting method, the method described above based on matching to either $t_{\max}$ or $t_{\min}$ is exact and completely deterministic. One final aspect of the free-stream velocity defined by Eq. (20) is that the zero down-crossing, t_0, occurs at $t_0=2\arccos(c)$, which is independent of b_1.

3.3. AOFT and generalised sawtooth free-stream velocity

Van der A et al. (2011) represented the normalised velocity and acceleration for a sawtooth wave in the Aberdeen Oscillating Flow Tunnel (AOFT) using

$$u(t)=f(b)\sum_{n=1}^{N}\frac{b^{n-1}}{n}\sin nt,\quad a(t)=f(b)\sum_{n=1}^{N}b^{n-1}\cos nt, \tag{24a, b}$$

where $f(b)$ ensures normalisation, such that $u_{\max}-u_{\min}=2$, and N is even. This description for the free-stream velocity, hereafter referred to as the AOFT description, isolates the effect of asymmetry from skewness, since $R=½$ and $\beta=(1+b)/2$. It was used to drive the oscillatory flow in the AOFT with $N=6$ for periods of 5 and 7 s, velocity amplitudes of 1–1.2 m/s and values of $\beta=0.5$, 0.6 and 0.75, see van der A et al. (2011). Since it is anticipated that asymmetry rarely occurs in isolation from skewness, the AOFT

description can be generalised to include both skewness and asymmetry by expressing the velocity and acceleration as

$$u = f(b,\varphi)\sum_{n=1}^{N}\frac{b^{n-1}}{n}\sin[nt+(1-n)\varphi], \tag{25a}$$

$$a = f(b,\varphi)\sum_{n=1}^{N}b^{n-1}\cos[nt+(1-n)\varphi], \tag{25b}$$

so that $\varphi=0$ corresponds to the AOFT description and $\varphi=\pi/2$ corresponds to a Stokes-type wave. Following the approach used by Abreu et al. (2010), Appendix F demonstrates that in the limit of $N=\infty$, Eqs. (25a,b) can be expressed

$$u = P_1 G(t), \quad a = 2bP_1\frac{\cos t - b\cos\varphi}{1+b^2-2b\cos(t-\varphi)}, \tag{26a, b}$$

where $G(t) = -\sin\varphi\log[1+b^2-2b\cos(t-\varphi)]+2\cos\varphi\arctan\{b\sin(t-\varphi)/[1-b\cos(t-\varphi)]\}$, log is the natural logarithm, $P_1=f/2b=2/[G(t_{m1})-G(t_{m2})]$, $t_{m1}=\arccos(b\cos\varphi)$ and $t_{m2}=2\pi-t_{m1}$. Eq. (26a,b) constitute a new description, referred to hereafter as the Generalised sawtooth (GSAW) description. When $\varphi=0$, the velocity and acceleration in the GSAW description are, respectively,

$$u = 2P_1\arctan\left[\frac{b\sin t}{1-b\cos t}\right], \quad a = 2P_1 b\frac{\cos t - b}{1+b^2-2b\cos t}, \tag{27a, b}$$

where $2P_1=1/\arctan[b(1-b^2)^{-½}]$ and $\beta=(1+b)/2$. Thus Eq. (27a,b) are the infinite-sum equivalents of Eq. (24a,b). A comparison between the AOFT (with $N=6$) and GSAW (with $\varphi=0$) descriptions is shown in Fig. 5 for $\beta=0.5$, 0.7 and 0.9 (for clarity only $0\le t\le\pi$ is shown). In general it can be seen that the AOFT approximation looses accuracy, by having too few harmonics, as β increases. Fig. 5 also shows GSAW accelerations. In the limit of $b\to1$ ($\beta\to1$), it follows that $2P_1=\pi^{-1}$ and $u=1-t/\pi$ for $0<t<2\pi$, and thus the GSAW description allows for the most extreme sawtooth shape possible. More generally, when $\varphi\neq0$, the GSAW description produces similar behaviour to that seen in Fig. 4 for the ABR description; but the details of this are discussed in Section 3.4.

3.3.1. GSAW skewness and asymmetry

For Eq. (26a,b) R, β and α can be expressed as

$$R = \frac{1}{2}u(t_{m1}),\ \beta = \frac{1}{2}(1+b\cos\varphi),\ \alpha = \frac{1}{\pi}[t_{m1}-\gamma], \tag{28a, b, c}$$

where $t_{m1}=\arccos(b\cos\varphi)$ and γ defines the zero up-crossing, corresponding to $u=0$ in Eq. (26a), which is a transcendental equation and so must be found either by interpolation or by using a Newton–Raphson technique, see Appendix F. For $\varphi=0$ or π, it follows that $\gamma=0$, $R=½$, $\beta=(1\pm b)/2$ and $\alpha=\pi^{-1}\arccos(\pm b)$ and, for $\varphi=\pm\pi/2$, it follows that $\gamma=\arcsin(\pm b/2)$, $R=\{\log[(1\mp b)/(1\pm b)]\}^{-1}\log(1\mp b)$, $\beta=½$ and $\alpha=\pi^{-1}\arccos(\pm b/2)$.

3.3.2. Fitting the GSAW description to observed velocities

As with the ABR description, the velocity for the GSAW description may be expressed as

$$u = P_1 G(t_1), \tag{29}$$

where $t_1=t+\gamma$. Thus for a given b and φ, it is necessary to determine γ as described above. In order to achieve a fitting procedure that is equivalent to that for the ABR description, it is first necessary to determine values of b and φ which correspond to a particular value of R. Even though the expression for R is exact, like that in the ABR description, this is more difficult to determine unless $\varphi=0$ ($R=½$). Firstly, since the maximum and minimum values of R for a given value of b correspond to $\varphi=\pm\pi/2$, the minimum value of b, b_{min}, for a given R can be determined from $R=\{\log[(1\pm b_{min})/(1\pm b_{min})]\}^{-1}\log(1\pm b_{min})$, for

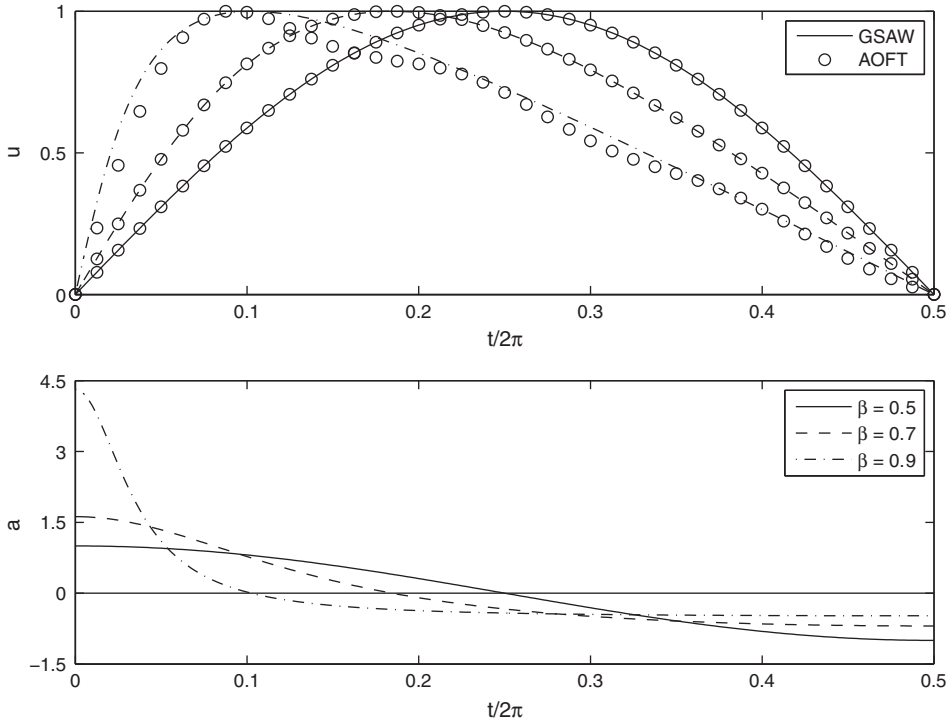

Fig. 5. (a) Comparison between the free-stream velocity for AOFT, Eq. (24a) with $N=6$, and GSAW, Eq. (26a) with $\varphi=0$, descriptions for the same values of β listed in panel b, (b) variation in the GSAW acceleration for selected values of β.

$R>½$ or $R<½$. This is a transcendental equation so requires either an interpolation or a Newton–Raphson step to be performed. Secondly, since rearranging Eq. (28a) in terms of either b or φ results in another transcendental equation, this requires a further interpolation/Newton–Raphson step to be performed in order to determine, say, the value of φ that corresponds to a given b and R. Performing these two steps results in all the allowable values of b ($b_{min}\le b\le 1$) and corresponding values of φ, on which a fitting procedure can be undertaken to find the optimum values of b and φ. The maximum and minimum values of the velocity will occur at $t_{max}=\arccos(b\cos\varphi)-\gamma$ and $t_{min}=2\pi-\arccos(b\cos\varphi)-\gamma$, respectively. However since γ requires an iterative procedure to determine it, unlike the ABR description, fitting on the basis of t_{max} or t_{min} is not really a feasible option so that b and φ need to be determined by some other method such as least-squares fitting. It is clear from the above explanation that, unless $\varphi=0$ or π, then fitting the GSAW description is more complicated than fitting the ABR description to an observed velocity time series.

3.4. Intercomparisons between the free-stream descriptions and other theoretical descriptions

3.4.1. Unskewed, asymmetric waves ($R=½$)

Fig. 6 shows a comparison for $\alpha=½$, ⅓ and ⅛ between the GSSO, ABR and the GSAW descriptions, Eqs. (10a,b), (16a,b) with $\varphi=0$ (for the GSSO description the case $\alpha=⅛$ is not possible). It can be seen that when $\alpha=½$ ($\beta=½$) all of the descriptions are identical. For the intermediate value $\alpha=⅓$, the velocities and accelerations for the ABR and GSAW descriptions are in reasonable agreement and this is reflected by identical values of $\beta=¾$, (identical values will result as long as $r<½$). However, the GSSO description already deviates quite substantially from the other two descriptions, because a value of $b=½$ is required in Eqs. (10a,b) to produce $\alpha=⅓$ ($\beta=16/25$). For the most extreme value of $\alpha=⅛$, the behaviour of the ABR and GSAW descriptions diverge ($\beta=0.877$ and 0.962, respectively). It can be seen that as α decreases (β increases), the concave behaviour of the ABR description as the flow decelerates after the crest becomes increasingly pronounced. According to Abreu et al. (2010) this concave nature is consistent with what was found by Elfrink et al. (2006), as seen in the next section. However, for $\varphi=0$, in the limit of $\alpha\to 0$ ($\beta\to 1$), it is only the GSAW and not the ABR description that has mathematically plausible behaviour [$u(t\neq 0,2\pi)=1-t/\pi$, $u(t=0,2\pi)=0$ for GSAW and $u(t\neq 0,2\pi)=0$, $u(t=0,2\pi)=\infty$ for ABR].

3.4.2. Skewed, symmetric waves ($\beta=½$)

Neither Drake and Calantoni (2001) nor Hsu and Hanes (2004) provided any physical argument for their choice of $b=½$ in Eq. (12a). Abreu et al. (2010) stated that their description with $\varphi=½\pi$ was a reasonable approximation to Cnoidal First-Order waves when $b<⅓$ ($R<⅔$, $r<0.6$) which is quite a stringent constraint since it does not include Drake and Calantoni's (2001) setting ($b=½$, $R=¾$). In order to re-examine this limit placed on the ABR description, it is of interest to determine the wave conditions under which the ABR free-stream velocity, Eq. (16a) with $b=½$ ($r=0.8$) and $\varphi=\pi/2$ might occur. This was done using Stream Function theory of Dalrymple (1974) directly from the website: http://www.coastal.udel.edu/faculty/rad/streamless.html, to tenth order. Here a number of water depths (h^*) and wave periods (T^*) were tested and then a wave height (H^*) was chosen which best matched $R=¾$. Fig. 7a shows the shapes of the Stream Function theory velocities compared with the ABR and GSAW descriptions with $R=¾$ and $\varphi=\pi/2$. It is clear that GSAW description is in worse agreement with the Stream Function theory velocities than the ABR description ($1-r_{sq}=2.3$–2.6% for GSAW compared with 0.36–0.5% for ABR, where r_{sq} is the r-squared value). For the ABR description, it can be seen that there is reasonable agreement in the shape, including the time of the zero down-crossing, but it tends to overpredict the acceleration near the crest and underpredict it near the trough (as demonstrated by the slopes of the curves). However, bearing in mind the simplicity of the ABR description, it is still a reasonable approximation. The values h^*, T^* and H^* required in Stream Function theory to produce these velocities are given in Table 2. When these values are plotted on h^*/g^*T^{*2} and H^*/g^*T^{*2} axes see Fig. 8a (Lé Méhauté, 1976), they collapse onto one curve and can all be classified as Cnoidal waves, as demonstrated by Abreu et al. (2010). Also from Stream Function theory for the cases

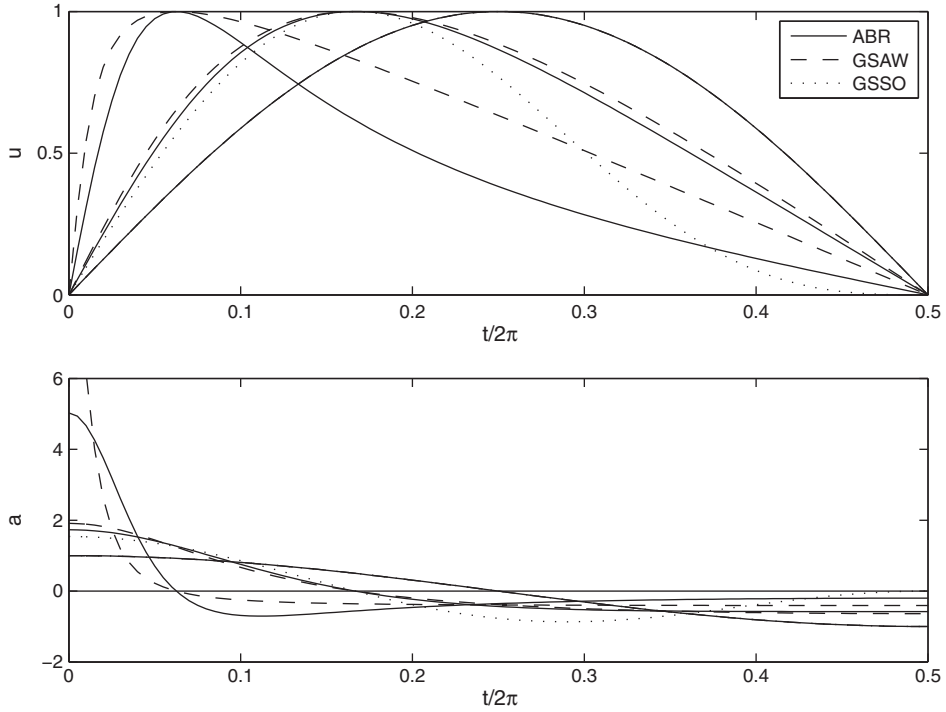

Fig. 6. Comparison between the free-stream velocity and acceleration for the GSSO, ABR and GSAW descriptions, Eqs. (10a,b), (16a,b) and (26a,b) with $\varphi=0$, for $\alpha=½$, ⅓ and ⅛ (for $\alpha=½$, all descriptions are identical and given by the solid line).

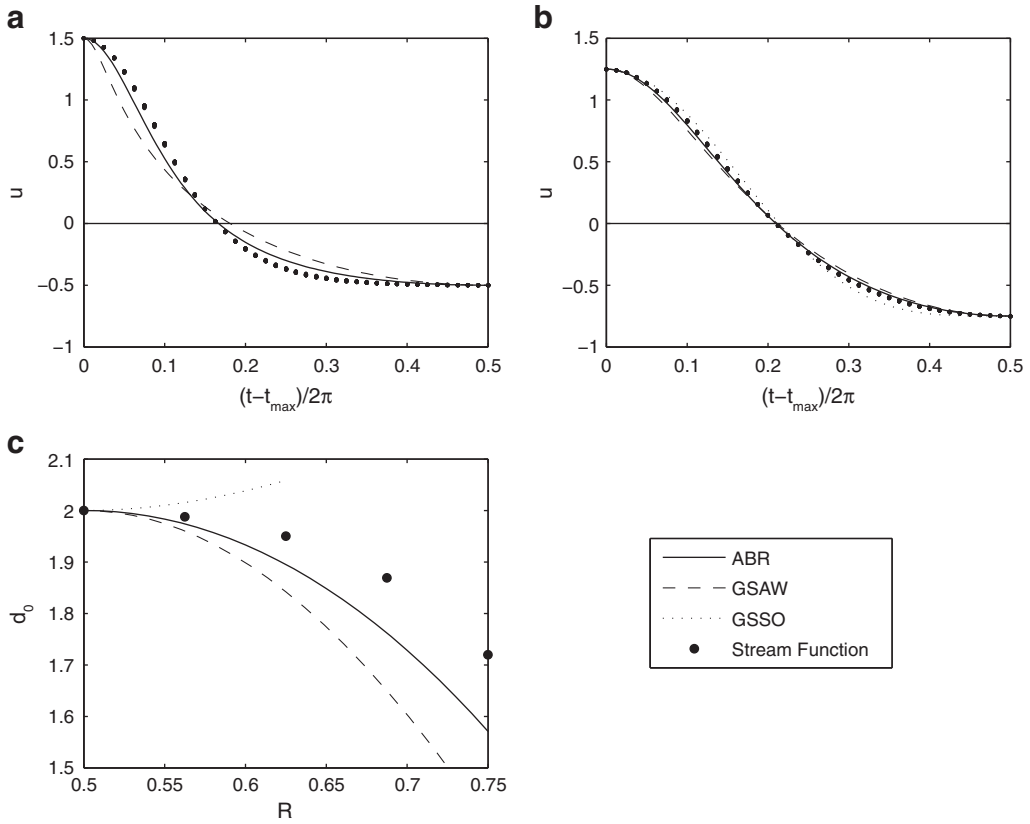

Fig. 7. Comparison between the ABR, GSAW and GSSO descriptions, with $\varphi = \frac{1}{2}\pi$, and tenth-order Stream Function theory. a) Velocity time series for $R = \frac{3}{4}$; b) velocity time series for $R = \frac{5}{8}$ and c) orbital diameter, d_0, and skewness R.

listed in Table 2, it was found that the normalisation velocity U_1^*/U_{Airy}^* collapses onto one curve, see Fig. 8b.

At the often assumed upper limit of skewness for the GSSO description ($R = \frac{5}{8}$), the Stream Function theory of Dalrymple (1974) was again used to determine the wave conditions under which this skewness occurs. The values h^*, T^* and H^* required in Stream Function theory to produce this value of R are given in Table 3. Again it can be seen in Fig. 8a and b that H^*/g^*T^{*2} and U_1^*/U_{Airy}^* collapse onto single curves. In Fig. 8a the curve corresponding to H^*/g^*T^{*2} is close to the Cnoidal/Stokes boundary but remains in the Cnoidal Regime according to the Lé Méhauté's (1976) classification. Fig. 7b shows a comparison between the shapes of these free-stream velocities with $R = \frac{5}{8}$ from Stream Function theory and the GSSO, ABR and GSAW descriptions, Eqs. (10a,b), (16a,b) and (26a,b) with $\varphi = \pi/2$. It is clear that for this smaller value of R there is less discrepancy between the descriptions and the Stream Function velocity than for the $R = \frac{3}{4}$ case, and this trend can be expected to continue as R decreases towards ½. Nevertheless, ABR still provides the best description; $1 - r_{sq} = 0.17$–0.22% for GSSO, 0.03–0.06% for ABR and 0.14–0.2% for GSAW.

Table 2
Wave heights in metres from Stream Function theory based on $R = \frac{3}{4}$.

T^* (s)	h^* 1	(m) 2	3	4
5	0.45	–	–	–
6	0.29	1.31	–	–
7	0.20	0.93	2.25	–
8	0.15	0.67	1.61	3.00
9	0.12	0.51	1.24	2.30
10	0.09	0.40	0.97	1.82

It is instructive to compare the free-stream velocities on the basis of their orbital diameter, d_0, which can be defined as (c.f. Fig. 1)

$$d_0 = \int_0^{t_0} u\,dt. \tag{30}$$

This is an important property of the wave since it determines how far a passive particle will be advected by the flow in half a wave cycle and is particularly relevant in determining ripple dimensions (see for example, O'Donoghue et al., 2006). A comparison between the variation of d_0 with R for the three different free-stream velocity descriptions with $\varphi = \pi/2$ and that determined by Stream Function theory is shown in Fig. 7c. The ABR and GSAW descriptions show the same trend as Stream Function theory where d_0 decreases with increasing R, but over predict it. The GSSO description on the other hand produces d_0 values that actually increase with R as has been noted by other authors (O'Donoghue et al., 2006). This apparent discrepancy is probably a reflection of the fact that a more stringent limit needs to be placed on b for the GSSO description. The ABR description produces d_0 values that are closest to those determined by Stream Function theory. Thus the ABR description, Eq. (16a) with $\varphi = \pi/2$, represents a reasonable compromise between the Cnoidal Wave and Stokes Wave descriptions.

3.5. Summary of findings

Based on the previous sections the ABR description provides the best and most versatile description of the free-stream velocity which includes both skewness and asymmetry, with the caveat that it cannot represent extreme asymmetry $\alpha \to 0$ ($\beta \to 1$), as discussed in Section 3.4.1. The ABR description provides a reasonable approximation to theoretical, symmetric descriptions and is simpler to use than the finite sum approximation of Drake and Calantoni (2001),

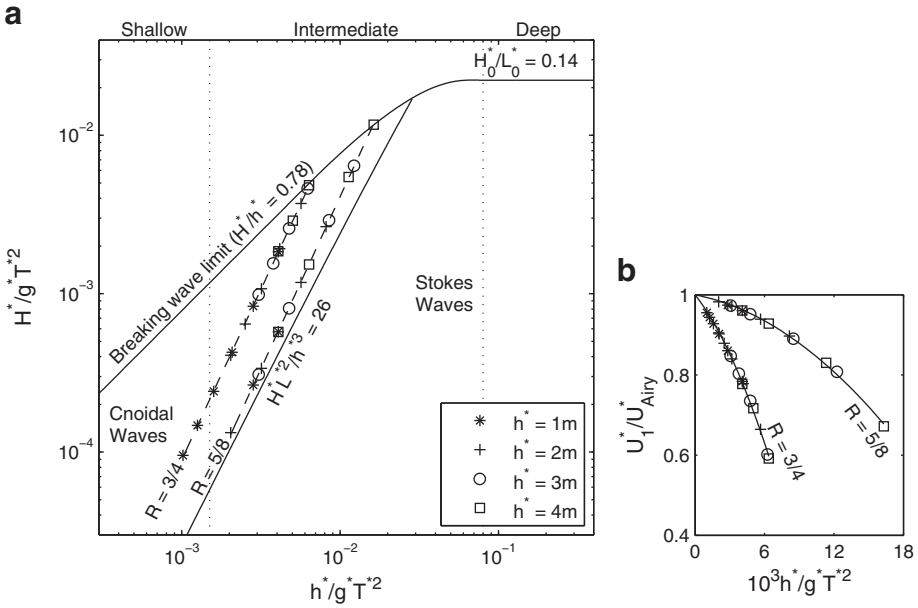

Fig. 8. Cases from Tables 2 and 3 ($R = ¾$ and ⅝) showing (a) Wave heights according to Lé Méhauté's (1976) classification and (b) normalisation velocity as a function of h^*/g^*T^{*2}.

because the normalisation, skewness and asymmetry measures and fitting procedures are more straightforward. Compared with the GSSO description, the ABR description is able to produce more skewness and asymmetry and, with the exception of β, has skewness and asymmetry parameters which are far less cumbersome to determine. For these reasons the ABR description is much the best suited to fitting to free-stream velocity data. However, in the case of extreme asymmetry and weak skewness it has been suggested that the newly developed GSAW description, which when $\varphi = 0$ is the infinite-sum equivalent to the AOFT description, is probably the best description to use even though it is more cumbersome. The ability of the ABR and GSAW descriptions to fit to observed data is tested in the next section.

4. Fitting the free-stream velocity to data

4.1. *Elfrink et al.'s (2006) description of free-stream velocity*

Elfrink et al.'s (2006) characterisation of the shape of the free-stream velocity, Eq. (6), is based on a large amount of irregular shoaling wave data from the field, so it is important that any potential velocity description can be well fitted to it. In the fitting of the ABR and GSAW descriptions to Elfrink's description, $U_1^*/U_{\mathrm{Airy}}^*$ and R can be determined directly using Eqs. (A1a,h) and (Ab,i). For the ABR description, since R appears explicitly in the Eq. (20), it is only necessary to determine b_1 either using $t_{\max}$, Eq. (A1c), or $t_{\min}$, Eq. (A1e), in Eq. (23) or by some other means as described in Section 3.2.1. Recall that because t_0 in Eq. (20) is only dependant on R it is not possible to fit on the basis of t_0. For the GSAW description, R determines the allowable values of b and φ, and the method for calculating these is explained in Section 3.3.2. Because of the complexity of fitting on the basis of $t_{\max}$ or $t_{\min}$ for the GSAW description, the most appropriate way to determine the optimum values of b and φ is by least-squares fitting.

In their paper, Elfrink et al. (2006) give example cases that cover the range of parameters over which their characterisation is valid. A selection of these cases, corresponding to the same range of conditions, is shown in Fig. 9 together with fits to the ABR description with b_1 based on least-squares fitting and matching to $t_{\max}$, $t_{\min}$, and to the GSAW description with b and φ based on least-squares fitting. The associated r_{sq} values are given in Table 4. Both descriptions are able to produce very good fits in all of the cases, including the representation of the concave nature of the flow as the flow accelerates after the maximum crest velocity. Based on least-squares fitting, the GSAW description produces a slightly better fit. However this has to be weighed against the fact that the ABR description is in closer agreement with symmetric wave theories, see Section 3.4.2, and is more straightforward to use. For the other fitting techniques used for the ABR description, while the b_1 based on least-squares fitting produces the best result, the b_1 based on $t_{\min}$ is the closest to this result. This is probably because $2\pi - t_{\min}$ is greater than $t_{\max}$, so that fitting to $t_{\min}$ produces a more representative b_1.

In light of this fitting it is now possible to re-examine how the free-stream velocity changes as normally-incident, waves shoal over a beach of constant slope, as discussed in Section 2.2, but this time with an acceleration which is continuous.

In Fig. 10 the cases of 5 and 7 s waves with deep-water heights, H_0^*, of 0.95 m are allowed to shoal over a beach slope of 1/40 with water depths ranging from 10 to 2 m without breaking and with H^* determined by linear theory. As in Fig. 2, it can be seen that both the skewness and asymmetry change simultaneously. In the case of the 5 s wave the continuous acceleration now produces more trustworthy values for β, than was the case in Fig. 2. In comparing the 5 and 7 s cases, it can be seen that the sharper increase in wave height for the 7 s wave results in a similar value of R but a greater value of β, compared with the 5 s case. The difference between the 5 and 7 s wave cases are the result of changes in the inputs to Elfrink et al.'s (2006) characterisation, Eq. (7a,b,c), and not the fitting. In this case the Elfrink velocity, Eq. (6), has been least-squares-fitted to the ABR

Table 3
Wave heights in metres from Stream Function theory based on $R = ⅝$.

T^* (s)	h^* 1	(m) 2	3	4
5	0.14	0.65	1.58	2.86
6	0.09	0.42	1.03	1.93
8	–	0.21	0.51	0.96
10	–	0.13	0.30	0.56

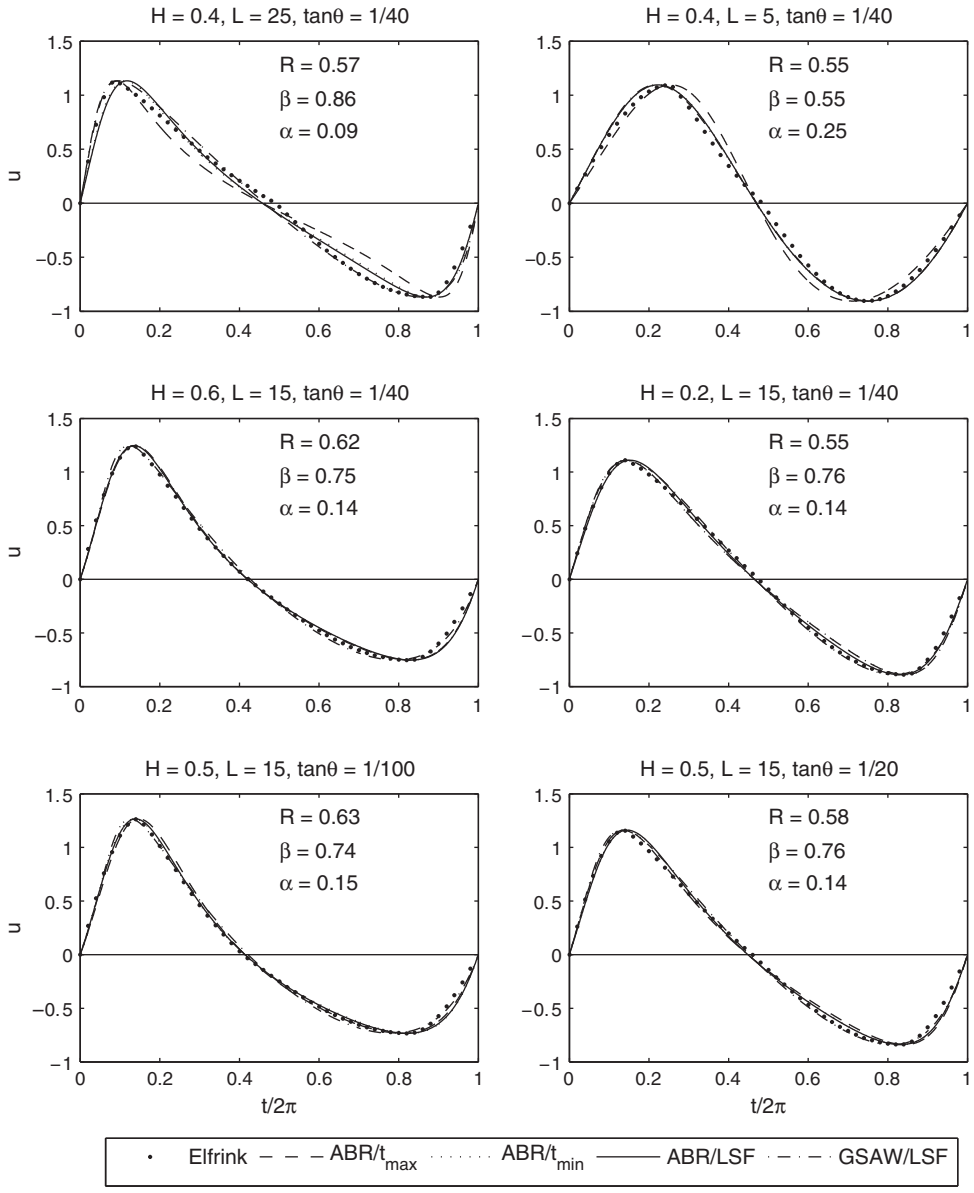

Fig. 9. Fit of ABR and GSAW descriptions, Eqs. (20) and (29), to Elfrink et al.'s (2006) example cases. For the ABR description the value of b is based on a matching to t_{max} and t_{min} (see Eq. (23)) and a least-squares fitting, and for GSAW the values of b and φ are found by least-squares fitting.

description (such that $1-r_{sq}$ was within 0.42% for both cases). However, in order to have a completely deterministic method, the fitting could have been carried out on the basis of u_{max} or u_{min}, such that skewness and asymmetry parameters can be related directly to the three physical wave and beach parameters, given by Eq. (7a,b,c).

Table 4
$1-r_{sq}$ values (as percentages) for the ABR and GSAW description fits shown in Fig. 9. Fits are based on a matching to t_{max}, t_{min}, and least-squares fitting (LSF).

Inputs		Description/fitting method				
H	L	1/tanθ	ABR/t_{max}	ABR/t_{min}	ABR/LSF	GSAW/LSF
0.4	25	40	3.05	1.01	0.98	0.43
0.4	5	40	1.83	0.29	0.28	0.26
0.6	15	40	0.33	0.33	0.33	0.17
0.2	15	40	0.41	0.44	0.18	0.10
0.5	15	100	0.36	0.29	0.26	0.24
0.5	15	20	0.51	0.36	0.36	0.15

4.2. Comparison with velocity data after waves have broken

Here Shin and Cox's (2006) data set is considered to examine the behaviour of the velocity time series after the waves have broken, in order to try to determine which of the previously discussed free-stream velocities is best suited to the case of comparatively strong asymmetry and weak skewness.

Shin and Cox (2006) performed very detailed measurements in the laboratory to examine the turbulence properties of the inner surf and swash zones. Waves with a period of 2 s were allowed to shoal on a beach. The beach consisted of two slopes: 1/35 offshore and a steeper slope of 1/10 inshore, to mimick the steepening of a typical foreshore. The offshore water depth and wave height were 0.60 and 0.11 m, respectively. On the 1/10 slope section the velocity tangential to the slope and the turbulence characteristics of the breaking wave were measured at two locations, E and I2, below and above the mean water line representing the inner surf zone and swash zone, respectively. Here, at E, $H=1.36$, $L=22$ and $\xi=0.76$

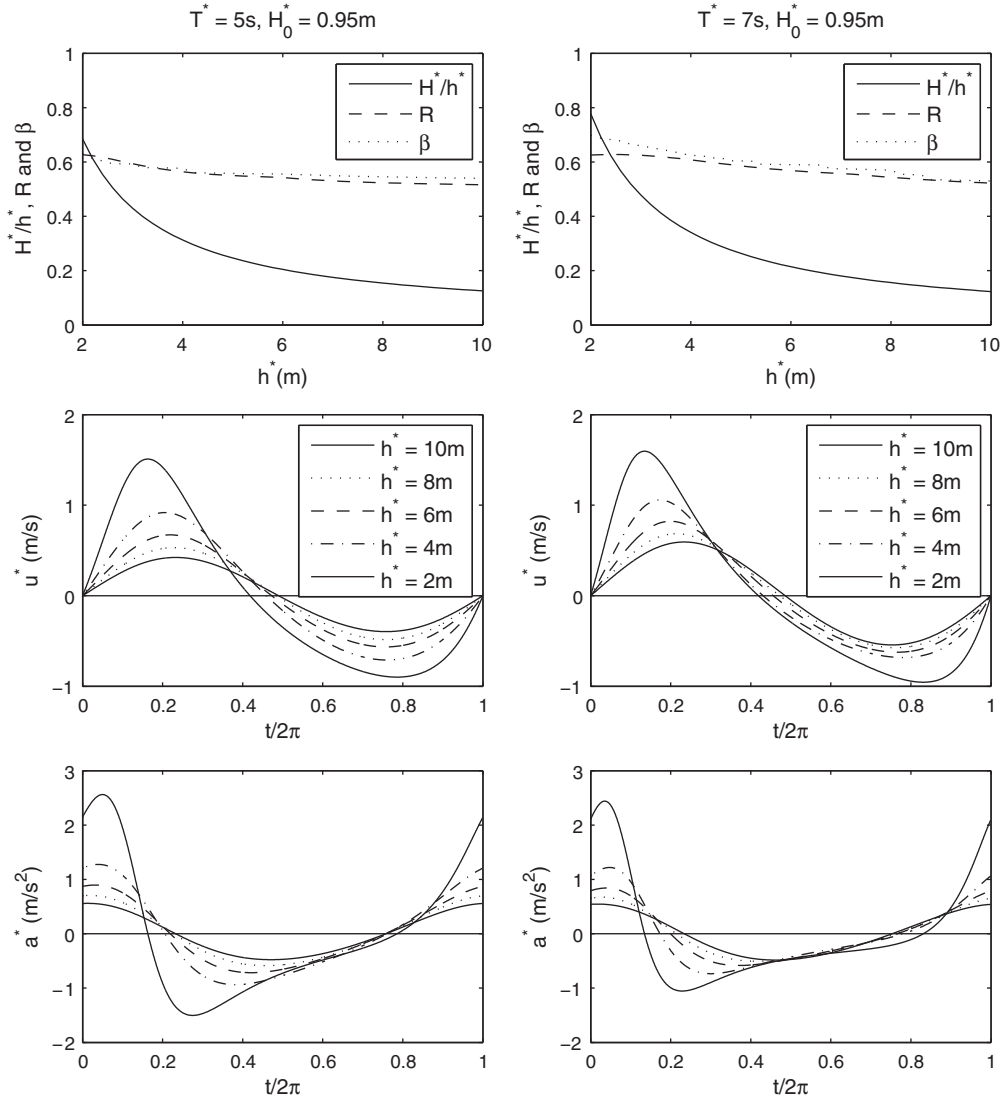

Fig. 10. Non-dimensional wave height, skewness and asymmetry and time series of the dimensional velocity and acceleration at selected heights for shoaling waves with periods of 5 and 7 s over a beach slope of 1/40 using the characterisation of Elfrink et al. (2006), based on fitting the ABR description.

and at I2, $H = 1.62$, $L = 41$ and $\xi = 1.29$, where H, L and ξ are defined in Eq. (7a,b,c). These values of H, L and ξ are both outside of the range considered by Elfrink et al. (2006).

The ABR and GSAW velocity descriptions are fitted to the tangential, phase-ensembled, free-stream velocity data from E and I2 at a height of 1.6 cm above the bed with the cycle mean velocity removed. The fits are shown in Fig. 11. At location E, it can be seen that the ABR description is much better suited to the velocity data, particularly in the way it represents the concave nature of the flow after the velocity maximum (as indicated by the relative r_{sq} values). At location I2, by contrast, the GSAW description produces the closer fit. This is partly because the skewness has reduced and asymmetry increased, so that the velocity is more sawtooth-like and therefore the GSAW description is better suited, but also because there is now no appreciable concave nature to the temporal variation in the flow. Thus it can be inferred that, when asymmetry dominates over skewness, the GSAW description is superior when the flow variation is not concave and the ABR description is superior when the flow variation is concave. However, bearing in mind the fact that the GSAW description is harder to fit than the ABR description, and that the GSAW only represents a modest improvement over the ABR description, the latter still represents the favoured description.

5. Discussion

In this paper, both the GSAW and ABR descriptions have been fitted to Elfrink et al.'s (2006) irregular wave characterisation and to regular wave data. The fitting techniques of the ABR description have been improved upon in this paper compared with the original procedure described by Abreu et al. (2010). Since the ABR description provides the best means to systematise skewness and asymmetry in the wave velocity, MATLAB scripts are provided to calculate the velocity and to fit it to data, see Appendix G. When these procedures are used together with the Elfrink et al. (2006) characterisation, which is also provided as a MATLAB script (see Appendices A and G), then from the inputs of H, L and ξ, see Eq. (7a,b,c), the quantities $U_1^*/U_{\mathrm{Airy}}^*$, R, $t_{\max}$, $t_{\min}$, t_0 and U_0 can be determined. Fitting to the ABR description on the basis of $t_{\max}$, $t_{\min}$ or a least-squares-fit, allows b_1 to be determined, such that the free-stream acceleration is continuous, and α, β and all the other measures of skewness and asymmetry can be calculated (see Table 1). These same fitting techniques can be applied to other characterisations.

For instance, Abreu et al. (2010) demonstrated that the ABR description can be fitted to the functional form of Isobe and Horikawa's (1982) characterisation

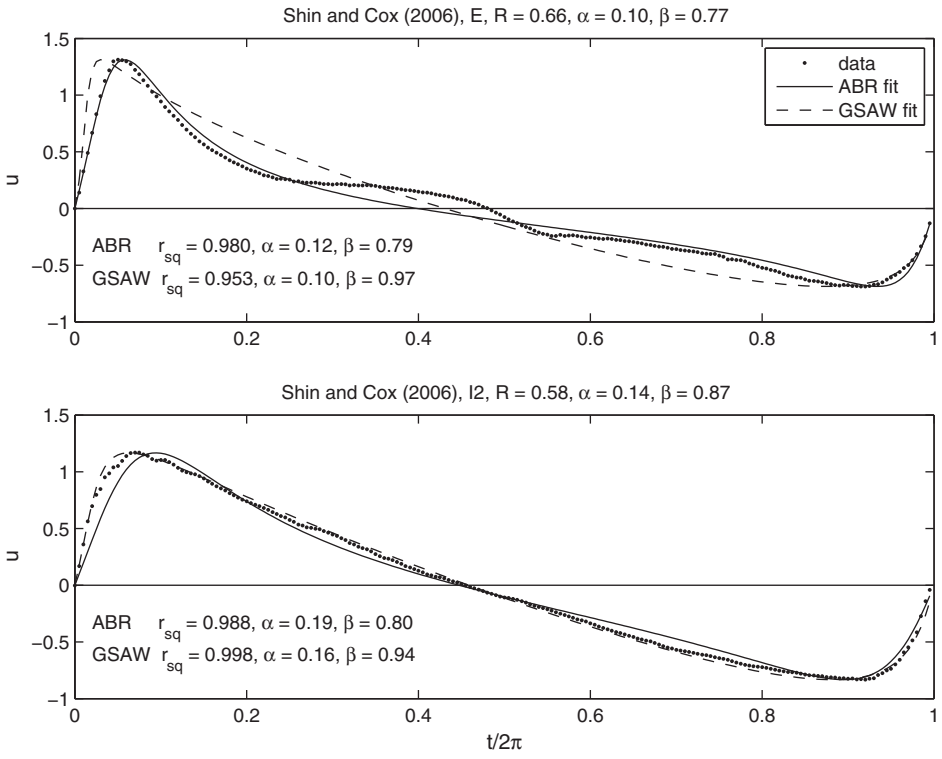

Fig. 11. Fit of the ABR and GSAW descriptions, Eqs. (20) and (29), to velocity time series from the laboratory data of Shin and Cox (2006).

$$u(t)=\begin{cases} 2R\sin\left[\dfrac{t}{2\alpha}\right], & -2\theta_2\le t<2(\alpha\pi-\theta_2), \\ 2(1-R)\sin\left[\dfrac{t-2\pi-2\theta_1}{2(1-\alpha)}\right], & 2(\alpha\pi-\theta_2)\le t<2(\pi-\theta_2), \end{cases} \tag{31}$$

where θ_1 and θ_2 are given by

$$\theta_1=(1-\alpha)\arcsin\sqrt{\frac{\mu_R^2\mu_\alpha^2-1}{\mu_R^2(\mu_\alpha^2-1)}}-\theta_2,\quad \theta_2=\alpha\arcsin\sqrt{\frac{\mu_R^2\mu_\alpha^2-1}{\mu_\alpha^2-1}},$$

and $\mu_R=(1-R)/R$ and $\mu_\alpha=(1-\alpha)/\alpha$. Eq. (31) is common to the characterisations of Dibajnia et al. (2001) and Grasmeijer and Ruessink (2003) (in case of Grasmeijer and Ruessink (2003) since α was not specified, $\alpha=1-R$). Eq. (31) has a zero mean, however when $R\neq\frac{1}{2}$, the acceleration is discontinuous at $t=2(\alpha\pi-\theta_2)$ and $2(\pi-\theta_2)$. Thus, as with Elfrink et al.'s (2006) characterisation, in order to fit the ABR description to the characterisations of Isobe and Horikawa (1982), Dibajnia et al. (2001) or Grasmeijer and Ruessink (2003) only requires fitting on the basis of b_1. b_1 can either be determined by least-squares fitting to Eq. (31) or, since $t_{max}=\alpha\pi$ and $t_{min}=(1+\alpha)\pi+2\theta_1$, it can be determined directly from Eq. (23). In the characterisations of Isobe and Horikawa (1982) and Dibajnia et al. (2001) U_1^*/U_{Airy}^*, R and α were determined by L, H, L_0, H_0/L_0 and tanθ, whereas in the Grasmeijer and Ruessink (2003) characterisation U_1^*/U_{Airy}^* and R were determined by L, H and L_0.

Fitting to irregular wave sequences on statistical grounds, by choosing a regular wave with equivalent skewness and/or asymmetry, has not been considered in this paper. Van Rijn et al. (2011) parameterised the skewness and asymmetry measures, A and S, in terms of the Ursell parameter, $Ur=HL^2$, and thus, as explained in Section 3.1.2, this is sufficient to determine φ, for any of the descriptions, and b when a particular description is considered, in a statistical sense (see for example, Ruessink et al., 2012).

Fitting to irregular wave sequences on a wave-by-wave basis, has also not been considered in this paper. However, the ability of the ABR description to fit to irregular waves sequences has already been demonstrated by Abreu et al. (2010). The procedure described in Section 3.2.2 can be generalised for this purpose, whereby the velocity and time between consecutive zero up-crossings are non-dimensionalised by the maximum and minimum in velocity and the individual wave period, respectively. Thus fitting only requires the determination of b_1 for each pair of zero up-crossings provided that the mean has been removed by high-pass filtering.

The improved fitting for the ABR description has allowed the phases and sizes of the maxima and minima in the free-stream velocity to be expressed exactly. Thus the calculation of the stress by, for example the method of Gonzalez-Rodriguez and Madsen (2007), which involves a time-varying friction factor and phase lead that vary between wave crest and trough values, could be applied more readily. The fact that phases and sizes of the maxima and minima can be expressed exactly is also potentially important in using the ABR description in a Dibajnia and Watanabe (1998) type sheet-flow sediment transport rate formulae, which is critically dependant on the relative sizes and timings of the velocity maximum and minimum.

6. Conclusions

This paper has reviewed the various free-stream velocity descriptions that have been used previously in the models and experiments to represent the skewness and asymmetry in waves. It has also quantified all the relevant measures of skewness and asymmetry for these descriptions. Building on the work of Abreu et al. (2010), it has been shown that their description (ABR) is able to represent most wave conditions in a relatively simple way. This description has been related to existing theoretical descriptions of skewed symmetric waves. For example, their description is far easier and better to use than the most obvious choice of a generalised Stokes second-order (GSSO) description. For waves with large asymmetry and small skewness, the observed temporal variation in velocities sometimes exhibits a concave

nature after the wave crest which is well captured by the ABR description. However, for situations where this is not the case an alternative description based on generalising the sawtooth shape (GSAW) has been developed in this paper.

It has also been shown that it is possible to fit the ABR description to an observed velocity, starting at the zero up-crossing, without any need for approximations by matching either the maximum or minimum in the velocity. When waves are both asymmetric and skewed, fitting on the basis of the minimum in the velocity has been found to be preferable. The ABR and GSAW descriptions fit well to Elfrink et al.'s (2006) description, which represents a large amount of irregular, shore-normal, shoaling-wave data prior to wave breaking. Thus it is possible to relate the physical and beach parameters of Elfrink et al. (2006) (non-dimensional wave height, wavelength and surf similarity parameter) directly to the measures of skewness and asymmetry. In this way both the ABR and GSAW descriptions are able to represent regular and irregular wave sequences in a model or wave tunnel in a systematic way. However, the ABR description remains the most simple to use and MATLAB scripts are provided for this description.

Acknowledgements

This work was partly funded by the UK Engineering and Physical Sciences Research Council (EPSRC) under the 'SANTOSS' project, GR/T28089 and partly by the UK Natural Environment Research Council (NERC) under the 'FORMOST' project, NE/E015123/1. Dr. Sungwon Shin, Oregon State University, is thanked for providing the velocity data for the shoaling-wave. Two anonymous reviewers are thanked for their constructive comments which improved the manuscript.

Appendix A. Elfrink et al.'s (2006) characterisation

Elfrink et al. (2006) determined that U_1^*, R, t_{max}, t_0 and t_{min} were given by

$$U_{1p}^* = U_{Airy}^*\left[A_1 + B_1 N_1\sqrt{\frac{L^{1/2} - \tanh|3\xi + 2L/Ur|}{UrN_1^2 + 1}}\right], \tag{A1a}$$

$$R_p = A_2 + B_2 H^{1/2}\left[1 - H^{1/2}\sqrt{|\xi| - \tanh(\tanh(|N_2|/Ur))}\right], \tag{A1b}$$

$$t_{max} = 2\pi[A_3 + B_3\tanh(C_3/N_3)], \tag{A1c}$$

$$t_{0p} = 2\pi\left[A_4 + B_4\left(H\tanh\left(C_4\xi L^3\right) - \tanh N_4\right)\right], \tag{A1d}$$

$$t_{min} = 2\pi\left[A_5 + \frac{B_5}{N_5 + N_6 + N_7 + N_8}\right], \tag{A1e}$$

where $A_1 = 0.5374$, $B_1 = 1.3921$, $A_2 = 0.38989$, $B_2 = 0.5366$, $A_3 = -0.0005$, $B_3 = -0.2615$, $C_3 = -9.3852$, $A_4 = 0.5028$, $B_4 = 0.0958$, $C_4 = 3.276\times10^{-4}$, $A_5 = 0.9209$, $B_5 = -2.3593$, $Ur = HL^2$, $N_1 = 2\xi(Ur/L)^{½} + 1$, $N_2 = \xi(11 - L) - |L - 10 - H + |\xi||$, $N_3 = \tanh(9.8496^2H^3L\xi^3) + \tanh(HL\xi) + L - 1$, $N_4 = H\tanh(3.5667\times10^{-4}\xi L^4)/\tanh[0.1206L\tanh(\tanh\xi)]$, $N_5 = [|L - Ur^{½} + (2.5185/L)^{½} - 4.4605|/H]^{½}$, $N_6 = |\xi| + \xi + L + 0.9206$, $N_7 = |1.1950\xi + 0.1950|L + (3.0176/H)^{½} - 5.2868 + H||$ and $N_8 = ||L + \xi| + |\xi| + \xi - 9.8976|$. Here the subscript p on U_{1p}^*, R_p and t_{0p}, indicates that they are provisional quantities, the significance of which is now explained. Elfrink et al. (2006) used the constraint that $\langle u\rangle = 0$ in Eq. (6) to determine U_{0p} (U_{0p} is also a provisional quantity), but also required $U_{0p} \le ½R_p$. The case when $U_{0p} = ½R_p$ requires t_{0p}, U_{1p}^*, R_p and U_{0p} to be adjusted, in order for $\langle u\rangle = 0$ to be maintained, and another variable, a_1, needed to be introduced. U_{0p} and a_1 are given by

$$U_{0p} = \min\left[\frac{R_p}{2}, \frac{2\left[t_{0p} - 2\pi(1 - R_p)\right]}{t_{0p} - t_{max}}\right], \tag{A1f}$$

$$a_1 = \max\left[\frac{0.99, U_{0p}t_{max} - 4\pi(1 - R_p)}{t_{0p}(U_{0p} - 2)}\right], \tag{A1g}$$

where $t_0 = a_1 t_{0p}$. When $U_{0p} \neq ½R_p$, $a_1 = 1$ and when $U_{0p} = ½R_p$, $a_1 < 1$. Thus U_1^*, R and U_0 can be expressed as

$$U_1^* = \begin{cases} U_{1p}^* \\ \left[\dfrac{2\pi - \frac{1}{4}(t_0 - t_{max})}{2\pi - t_0}\right] R_p U_{1p}^*, \end{cases} \quad R = \begin{cases} R_p, \\ \dfrac{2\pi - t_0}{2\pi - \frac{1}{4}(t_0 - t_{max})}, \end{cases} \tag{A1h, i}$$

$$U_0 = \begin{cases} U_{0p}, a_1 = 1, \\ \dfrac{R}{2}, \quad a_1 < 1. \end{cases} \tag{A1j}$$

A MATLAB script of this characterisation, elfrinknd.m, is provided at http://pages.bangor.ac.uk/~oss101/jmSA.html (see also Appendix G). This script takes t ($0 \le t < 2\pi$), H, L and ξ as inputs and returns U_1^*/U_{Airy}^*, R, t_{max}, t_0, t_{min} and U_0 and u and a (evaluated at t).

Appendix B. Quartic solution

Expressions for f, R and β for Eqs. (10a,b) and the expression for β for Eqs. (13b) or (16b) are all determined by a quartic equation

$$B_4x^4 + B_3x^3 + B_2x^2 + B_1x + B_0 = 0. \tag{B1}$$

For Eqs. (10a,b), both R and f depend on the positions of u_{max} and u_{min}, t_{m1} and t_{m2}. t_{m1} and t_{m2} are determined from Eq. (10b): $a(t_{mn}) = 0$, or $\cos t_{mn} + 2b\cos(2t_{mn} - \varphi) = 0$, which results in a quartic equation in $x_m = \cos t_{m1}$ or $\cos t_{m2}$, where $B_4 = 1$, $B_3 = \cos\varphi/2b$, $B_2 = (4b)^{-2} - 1$, $B_1 = -½B_3$ and $B_0 = B_3^2b^2$. Then $R = ½fu(t_{m1})$ and $f = 2/[u(t_{m1}) - u(t_{m2})]$, where t_{m1} and t_{m2} are the phases when max $[u(\arccos x_m)]$ and $\min[u(2\pi - \arccos x_m)]$ occur, u is given by Eq. (10a) with $f = 1$ and x_m are the real roots ($|x_m| \le 1$) of Eq. (B1). An expression for β can be derived in a similar way using Eq. (2b) with $a_{max} = \max[a(t_{mn})]$ and $a_{min} = \min[t_{mn})]$, where $a(t)$ is given by Eq. (10b) with $f = 1$, t_{mn} is given by

$$t_{mn} = \begin{cases} \arccos x_m, & 0 \le \varphi \le \pi, \\ 2\pi - \arccos x_m, & -\pi < \varphi < 0, \end{cases} \tag{B2}$$

and x_m are the real roots of Eq. (B1) with $B_4 = 1$, $B_3 = \cos\varphi/4b$, $B_2 = 1/(8b)^2 - 1$, $B_1 = -B_3$ and $B_0 = (16\sin^2\varphi - b^{-2})/64$, based on the derivative of Eq. (10b) $\sin t_{mn} + 4b\sin(2t_{mn} - \varphi) = 0$. Determining an expression for α is even more cumbersome since it requires both t_{m1}, from the R and f calculation, and γ (the phase when $u = 0$) to be found because $\alpha = (t_{m1} - \gamma)/\pi$. In the case of the latter $\gamma = \arccos x_m$, where x_m is a real root of Eq. (B1) with $B_4 = 1$, $B_3 = \cos\varphi/b$, $B_2 = (2b)^{-2} - 1$, $B_1 = -B_3$ and $B_0 = (\sin^2\varphi - b^{-2})/4$ occurring after u_{min} and before u_{max}.

Following the same procedure as above for the acceleration, based on the derivative of Eq. (13b), the exact general expression for β is given by Eq. (2b) with $a_{max} = \max[a(t_{mn})]$ and $a_{min} = \min[a(t_{mn})]$, where $a(t)$ is given by Eq. (13b), t_{mn} is given by Eq. (B2) and x_m are real roots ($|x_m| \le 1$) that satisfy Eq. (B1) with $B_4 = r^2(1 - r^2\sin^2\varphi)$, $B_3 = 2r\cos\varphi[1 - 2r^2 + r^2(1 - 2P)\sin^2\varphi]$, $B_2 = 6Pr^2\sin^2\varphi[1 - (1 - P)\sin^2\varphi] + 4P^4 - 3P^2$, $B_1 = -2r\cos\varphi[1 - 2r^2\cos^2\varphi + (2 - 3r^2 - 2P^3)\sin^4\varphi]$ and $B_0 = (1 - P)\sin^2\varphi[-1 - 3P + 4r^2 + 4Pr^2 - (1 - P + 2r^2)\sin^2\varphi + r^2(1 - P)\sin^4\varphi] + 4r^2P^2 - 1$, where $P = (1 - r^2)^{½}$. Substituting $r = 2b/(1 + b^2)$ and $c = b\sin\varphi$ and $b_1(1 - c^2/b_1^2)^{½} = b\cos\varphi$, where $c = 2R - 1$, allows $B_{4\text{-}0}$ to be expressed entirely in terms of b and φ or R and b_1.

Appendix C. Expressions for u^*_{spike}, a^*_{spike}, S, A_a and A

This appendix derives u^*_{spike}, a^*_{spike}, S, A_a and A by first determining $\langle u^2\rangle$, $\langle a^2\rangle$, $\langle u^3\rangle$, $\langle \tilde{u}^3\rangle$ and $\langle a^3\rangle$ for the different free-stream velocities. The velocity and acceleration can be expressed generically as

$$u=\sum_{n=1}^{N} B_n \sin(n\theta+\varphi),\quad a=\sum_{n=1}^{N} nB_n \cos(n\theta+\varphi), \tag{C1a, b}$$

where $\theta=t-\varphi$. It can be shown that $\langle u^2\rangle$ and $\langle a^2\rangle$ can be expressed as

$$\langle u^2\rangle=\frac{1}{2}\sum_{n=1}^{N} B_n^2,\quad \langle a^2\rangle=\frac{1}{2}\sum_{n=1}^{N} n^2 B_n^2, \tag{C2a, b}$$

and, since the Hilbert transform of $\sin(n\theta+\varphi)=-\cos(n\theta+\varphi)$, $\langle u^3\rangle$ and $\langle \tilde{u}^3\rangle$ can be expressed as

$$\langle u^3\rangle=\frac{3}{4}\sin\varphi\sum_{n=2}^{N} B_n\sum_{m=1}^{n-1} B_m B_{n-m}, \tag{C2c}$$

$$\langle \tilde{u}^3\rangle=-\frac{3}{4}\cos\varphi\sum_{n=2}^{N} B_n\sum_{m=1}^{n-1} B_m B_{n-m}, \tag{C2d}$$

and $\langle a^3\rangle$ can be expressed as

$$\langle a^3\rangle=\frac{3}{4}\cos\varphi\sum_{n=2}^{N} nB_n\sum_{m=1}^{n-1} m(n-m)B_m B_{n-m}. \tag{C2e}$$

For Eq. (8a,b), $N=2$, $\varphi=\pi/2$ and $B_n=fb^{n-1}$ in Eqs. (C2a,b,c,d,e), so that $\langle u^2\rangle=(1+b^2)/2$, $\langle a^2\rangle=(1+4b^2)/2$, $\langle u^3\rangle=3b/4$ and $\langle \tilde{u}^3\rangle=\langle a^3\rangle=0$, which when substituted into Eqs. (3a,b) and (4a,b,c) give

$$\frac{u^*_{spike}}{U_1^*}=\frac{3b}{2(1+b^2)},\quad \frac{a^*_{spike}}{A_1^*}=0, \tag{C3a, b}$$

$$S=\frac{3b}{\sqrt{2(1+b^2)^3}},\quad A=0,\quad A_a=0. \tag{C3c, d, e}$$

For Eqs. (10a,b), $N=2$ and $B_n=fb^{n-1}$ in Eqs. (C2a,b,c,d,e), so $\langle u^2\rangle=f^2(1+b^2)/2$, $\langle a^2\rangle=f^2(1+4b^2)/2$, $\langle u^3\rangle=3bf^3\sin\varphi/4$, $\langle a^3\rangle=3bf^3\cos\varphi/2$ and $\langle \tilde{u}^3\rangle=-3bf^3\cos\varphi/4$, these can be substituted into Eqs. (3a,b) and (4a,b,c) to give

$$\frac{u^*_{spike}}{U_1^*}=\frac{3bf\sin\varphi}{2(1+b^2)},\quad \frac{a^*_{spike}}{A_1^*}=\frac{3bf\cos\varphi}{1+4b^2}, \tag{C4a, b}$$

$$S=\frac{3b\sin\varphi}{\sqrt{2(1+b^2)^3}},\quad A=-\frac{3b\cos\varphi}{\sqrt{2(1+b^2)^3}}, \tag{C4c, d}$$

$$A_a=3b\sqrt{\frac{2}{(1+4b^2)^3}}\cos\varphi. \tag{C4e}$$

Eq. (C4c,d) are equivalent to the expressions for S and A quoted by van Rijn et al. (2011). For Eqs. (12a), (12b), $B_n=fb^{n-1}$ in Eqs. (C2a,b,c,d), so that $\langle u^2\rangle$, $\langle a^2\rangle$, $\langle u^3\rangle$ and $\langle \tilde{u}^3\rangle$ are

$$\langle u^2\rangle=\frac{f^2}{2b}S_0^N,\quad \langle a^2\rangle=\frac{f^2}{2b}S_2^N, \tag{C5a, b}$$

$$\langle u^3\rangle=\frac{3}{4}f^3\sin\varphi\sum_{n=2}^{N}(n-1)b^{2n-3}=\frac{3}{4}f^3\sin\varphi S_1^{N-1}, \tag{C5c}$$

$$\langle \tilde{u}^3\rangle=-\frac{3}{4}f^3\cos\varphi S_1^{N-1}, \tag{C5d}$$

where

$$S_m^N=\sum_{n=1}^{N} n^m b^{2n-1},$$

and various S_m^N are defined in Appendix D. From Eq. (C2e) $\langle a^3\rangle$ can be expressed as

$$\langle a^3\rangle=\frac{3f^3}{4}\cos\varphi\sum_{n=2}^{N} b^{2n-3}\sum_{m=1}^{n-1} n^2m-nm^2=\frac{f^3}{8b^2}\cos\varphi\left(S_4^N-S_2^N\right). \tag{C5e}$$

From Eqs. (C5a,b,c,d,e) using geometric series with $N=\infty$ (see Appendix D) and $f=1-b^2$ allows $\langle u^2\rangle$, $\langle a^2\rangle$, $\langle u^3\rangle$, $\langle \tilde{u}^3\rangle$ and $\langle a^3\rangle$ for Eqs. (16a,b) to be given exactly by

$$\langle u^2\rangle=\frac{1}{2}(1-b^2),\quad \langle a^2\rangle=\frac{1+b^2}{2(1-b^2)}, \tag{C6a, b}$$

$$\langle u^3\rangle=\frac{3}{4}b(1-b^2)\sin\varphi,\quad \langle \tilde{u}^3\rangle=-\frac{3}{4}b(1-b^2)\cos\varphi \tag{C6c, d}$$

$$\langle a^3\rangle=\frac{3(1+b^2)}{2(1-b^2)^2}b\cos\varphi. \tag{C6e}$$

Substituting Eqs. (C6a,b,c,d,e) into Eqs. (3a,b) and (4a,b,c) results in

$$\frac{u^*_{spike}}{U_1^*}=\frac{3}{2}b\sin\varphi,\quad \frac{a^*_{spike}}{A_1^*}=\frac{3b\cos\varphi}{1-b^2}, \tag{C7a, b}$$

$$S=\frac{3b\sin\varphi}{\sqrt{2(1-b^2)}},\quad A=-\frac{3b\cos\varphi}{\sqrt{2(1-b^2)}}, \tag{C7c, d}$$

$$A_a=\frac{3\sqrt{2}b\cos\varphi}{\sqrt{1-b^4}}, \tag{C7e}$$

and with the substitution $c=b\sin\varphi$ and $b_1(1-c^2/b_1^2)^{1/2}=b\cos\varphi$, these can be written

$$\frac{u^*_{spike}}{U_1^*}=\frac{3}{2}c,\quad \frac{a^*_{spike}}{A_1^*}=\frac{3b_1\sqrt{1-c^2/b_1^2}}{1-b_1^2} \tag{C8a, b}$$

$$S=\frac{3c}{\sqrt{2(1-b_1^2)}},\quad A=-3b_1\sqrt{\frac{1-c^2/b_1^2}{2(1-b_1^2)}}, \tag{C8c, d}$$

$$A_a=3b_1\sqrt{\frac{2(1-c^2/b_1^2)}{1-b_1^4}}, \tag{C8e}$$

where $c=2R-1$.

For Eqs. (25a,b), $B_n=fb^{n-1}/n$ in Eqs. (C2a,b,c,d,e), so that $\langle u^2\rangle$, $\langle a^2\rangle$, $\langle u^3\rangle$, $\langle \tilde{u}^3\rangle$ and $\langle a^3\rangle$ are

$$\langle u^2\rangle=\frac{1}{2b^2}f^2\sum_{n=2}^{N}\frac{b^{2n}}{n^2},\quad \langle a^2\rangle=\frac{1}{2b}f^2S_0^N, \tag{C9a, b}$$

$$\langle u^3\rangle = \frac{3f^3}{2b^3}\sin\varphi\sum_{n=2}^{N}\frac{b^{2n}}{n^2}\sum_{m=1}^{n-1}\frac{1}{m}, \tag{C9c}$$

$$\langle \tilde{u}^3\rangle = -\frac{3f^3}{2b^3}\cos\varphi\sum_{n=2}^{N}\frac{b^{2n}}{n^2}\sum_{m=1}^{n-1}\frac{1}{m}, \tag{C9d}$$

$$\langle a^3\rangle = \frac{3}{4}f^3\cos\varphi S_1^{N-1}, \tag{C9e}$$

Again from Eqs. (C9a,b,c,d,e) using geometric series with $N=\infty$ and $f=2P_1b$, allows $\langle u^2\rangle$, $\langle a^2\rangle$, $\langle u^3\rangle$, $\langle \tilde{u}^3\rangle$ and $\langle a^3\rangle$ for Eq. (24a,b) to be given exactly by

$$\langle u^2\rangle = 2P_1^2 Li_2(b^2), \quad \langle a^2\rangle = \frac{2P_1^2b^2}{1-b^2}, \tag{C10a, b}$$

$$\langle u^3\rangle = 12P_1^3X(b)\sin\varphi, \quad \langle \tilde{u}^3\rangle = -12P_1^3X(b)\cos\varphi, \tag{C10c, d}$$

$$\langle a^3\rangle = \frac{6P_1^3b^4\cos\varphi}{(1-b^2)^2}, \tag{C10e}$$

where Li_2 is the dilogarithm function and $X(b)$ is given by

$$X(b) = \sum_{n=2}^{\infty}\frac{b^{2n}}{n^2}\sum_{m=1}^{n-1}\frac{1}{m}, \tag{C11}$$

see Appendix D. Substituting Eqs. (C10a,b,c,d,e) into Eqs. (3a,c) and (4a,b,c) gives

$$\frac{u^*_{spike}}{U_1^*} = \frac{6P_1X(b)\sin\varphi}{Li_2(b^2)}, \quad \frac{a^*_{spike}}{A_1^*} = \frac{3P_1b^2\cos\varphi}{1-b^2}, \tag{C12a, b}$$

$$S = \frac{3\sqrt{2}X(b)\sin\varphi}{Li_2^{1.5}(b^2)}, \quad A = -\frac{3\sqrt{2}X(b)\cos\varphi}{Li_2^{1.5}(b^2)}, \tag{C12c, d}$$

$$A_a = \frac{3b\cos\varphi}{\sqrt{2(1-b^2)}}. \tag{C12e}$$

Appendix D. Geometric series

Most of the geometric series used in this paper can be expressed generically as

$$S_m^N = \sum_{n=1}^{N} n^m b^{2n-1}, \tag{D1}$$

where $N>1$. It can be shown that S_0^N, S_1^N, S_2^N, S_3^N and S_4^N are given by

$$S_0^N = \frac{b-b^{2N+1}}{1-b^2}, \quad S_1^N = \frac{S_0^N - Nb^{2N+1}}{1-b^2}, \tag{D2a, b}$$

$$S_2^N = \frac{2S_1^N - S_0^N - N^2b^{2N+1}}{1-b^2}, \tag{D2c}$$

$$S_3^N = \frac{3S_2^N - 3S_1^N + S_0^N - N^3b^{2N+1}}{1-b^2}, \tag{D2d}$$

$$S_4^N = \frac{4S_3^N - 6S_2^N + 4S_1^N - S_0^N - N^4b^{2N+1}}{1-b^2}. \tag{D2e}$$

For $N=\infty$, Eqs. (D2a,b,c,d,e) can be expressed more simply as $b/(1-b^2)$, $b/(1-b^2)^2$, $b(1+b^2)/(1-b^2)^3$, $b(1+4b^2+b^4)/(1-b^2)^4$ and $b(1+11b^2+11b^4+b^6)/(1-b^2)^5$. The other remaining infinite geometric series used in this paper are polylogarithms and $X(b)$

$$Li_k(b) = \sum_{n=1}^{\infty}\frac{b^n}{n^k}, \quad X(b) = \sum_{n=2}^{\infty}\frac{b^{2n}}{n^2}\sum_{m=1}^{n-1}\frac{1}{m}. \tag{D3a, b}$$

where $k=1$ or 2. For $k=1$, $\mathrm{Li}_1(b) = -\log(1-b)$ and for $k=2$, $\mathrm{Li}_2(b)$ is known as the dilogarithm. For $0\le b\le 1$, $\mathrm{Li}_2(b)$ can be approximated to within 1 and 0.1% of its true value by truncating the series at $n=70$ and 700, respectively. For $0\le b\le 1$, $X(b)$ can be approximated to within 1 and 0.1% of its true value by truncating the series at $n=700$ and 10,000, respectively.

Appendix E. Determining $f(b,\varphi)$ and R for Eq. (16a)

From the expression for the acceleration, Eq. (16b), the condition for the phase of the maximum and minimum in velocity can be expressed as

$$(1+b^2-2c^2)\cos t_m = \pm 2\sqrt{b^2-c^2}(1-c\sin t_m), \tag{E1}$$

where $c=b\sin\varphi$ and t_m is the phase of the maximum or minimum. Eq. (E1) can be expressed as a quadratic in $\sin t_m$

$$\left[(1+b^2)2-4c^2\right]\sin^2 t_m - 8c(b^2-c^2)\sin t_m - \left[(1-b^2)2+4c^4-4b^2c^2\right] = 0, \tag{E2}$$

which has solutions given by

$$\sin t_m = \frac{4c(b^2-c^2)\pm(1-b^2)(1+b^2-2c^2)}{(1+b^2)^2-4c^2,} \tag{E3}$$

where the positive/negative roots correspond to the maximum/minimum. From the expression for the velocity, Eq. (16a), the maximum/minimum can be written as

$$u_{\max/\min} = \frac{f(b,\varphi)(\sin t_m - c)}{1+b^2-2c\sin t_m \mp 2\sqrt{b^2-c^2\cos t_m}}, \tag{E4}$$

and substituting Eq. (E1) into Eq. (E4) and simplifying allows $u_{\max/\min}$ to be expressed as

$$u_{\max/\min} = \frac{f(1+b^2-2c^2)(\sin t_m - c)}{(1-b^2)(1-b^2+2c^2-2c\sin t_m)}. \tag{E5}$$

Finally substituting $\sin t_m$ from Eq. (E3) into Eq. (E5) and simplifying gives $u_{\max/\min} = \pm f(1\pm c)/(1-b^2)$. Since $u_{\max}-u_{\min} = 2f/(1-b^2)$, normalisation requires that $f(b,\varphi) = 1-b^2$, this allows $R = u_{\max}/2$, $u_{\max} = 1+c = 1+b\sin\varphi$ and therefore $R = (1+b\sin\varphi)/2$ or $b\sin\varphi = 2R-1$.

Appendix F. Proof that Eqs. (25a,b) when $N=\infty$ are equivalent to Eq. (26a,b)

From Eq. (25a), assuming that $N=\infty$, the velocity is

$$u = f(b,\varphi)\sum_{n=1}^{\infty}\frac{b^{n-1}}{n}\sin[nt+(1-n)\varphi], \tag{F1}$$

and following the approach of Abreu et al. (2010) of expressing the velocity, Eq. (F1), as a complex geometric series

$$u = f\mathrm{Im}\left\{\sum_{n=1}^{\infty}\frac{b^{n-1}}{n}e^{i[nt+(1-n)\varphi]}\right\} = \frac{f}{b}\mathrm{Im}\left\{e^{i\varphi}\sum_{n=1}^{\infty}\frac{\left(be^{i(t-\varphi)}\right)^n}{n}\right\}$$
$$= \frac{f}{b}\mathrm{Im}\left\{-e^{i\varphi}\log\left(1-be^{i(t-\varphi)}\right)\right\}, \quad \text{(F2)}$$

where $i=(-1)^{½}$ and Im represents the imaginary part (the real part corresponds to $-\tilde{u}$). Thus, u may be expressed as

$$u = \frac{f}{b}\mathrm{Im}\left\{\begin{array}{l} -\frac{1}{2}e^{i\varphi}\log\left(1-2b\cos(t-\varphi)+b^2\right) \\ \quad +ie^{i\varphi}\arctan\left[\frac{b\sin(t-\varphi)}{1-b\cos(t-\varphi)}\right]\end{array}\right\} = P_1 G(t), \quad \text{(F3)}$$

where $P_1=f/2b$ and $G(t)=-\sin\varphi\log[1+b^2-2b\cos(t-\varphi)]+2\cos\varphi\arctan\{b\sin(t-\varphi)/[1-b\cos(t-\varphi)]\}$, and therefore a may be expressed as

$$a = f\frac{\cos t - b\cos\varphi}{1+b^2-2b\cos(t-\varphi)}. \quad \text{(F4)}$$

From Eq. (F4) it can be seen that $u_{\max}$ and $u_{\min}$ occur at $\cos t_{mn}=b\cos\varphi$, so that $t_{m1}=\arccos(b\cos\varphi)$ and $t_{m2}=2\pi-t_{m1}$, now since $u_{\max}-u_{\min}=P_1[G(t_{m1})-G(t_{m2})]=2$, $P_1=2/[G(t_{m1})-G(t_{m2})]$. In order to determine γ the (the phase where $u=0$ in Eq. (F3)) requires the solution to a transcendental equation. This can either be found using interpolation or more accurately using the Newton–Raphson technique. For the Newton–Raphson technique: $\gamma_{n+1}=\gamma_n-u(\gamma_n)/a(\gamma_n)$ where γ_n is the n_{th} estimate of γ. Thus to begin at the zero up-crossing, t in Eqs. (F3) and (F4) must be replaced by $t+\gamma$.

When $\varphi=0$ and $\gamma=0$, $2P_1=1/\arctan[b(1-b^2)^{-½}]$, the velocity and acceleration can be expressed

$$u = 2P_1\arctan\left[\frac{b\sin t}{1-b\cos t}\right], \quad a = 2P_1 b\frac{\cos t-b}{1+b^2-2b\cos t}. \quad \text{(F5a, b)}$$

Eq. (F5a) may also be expressed as $u=P_1[\pi-t-2\arctan(P_0\cot ½t)]$, where $P_0=(1-b)/(1+b)$, so that in the limit of $b=1$, $P_1=1/\pi$ and therefore $u=1-t/\pi$, $a=-1/\pi$ for $0<t<2\pi$. When $\varphi=\pi/2$, $t_{m1}=\pi/2$ and $t_{m2}=3\pi/2$, $P_1=\{\log[(1+b)/(1-b)]\}^{-1}$.

R and α can readily be expressed as

$$R = \frac{1}{2}u(t_{m1}), \quad \alpha = \frac{1}{\pi}[t_{m1}-\gamma], \quad \text{(F6a, b)}$$

and since the expression for a given Eq. (F4) is exactly equivalent to the expression for u given by Eq. (16a), except that cosine replaces sine, it can be shown that since Eq. (16a) results in $R=(1+b\sin\varphi)/2$ so for Eq. (F4) β is given by

$$\beta = \frac{1}{2}(1+b\cos\varphi), \quad \text{(F6c)}$$

using an analogous argument to that given in Appendix E. It can be seen that when $\varphi=0$ or π, $\gamma=0$, $R=½$, $\beta=(1\pm b)/2$ and $\alpha=\pi^{-1}\arccos(\pm b)$ and when $\varphi=\pm\pi/2$, $\gamma=\arcsin(\pm b/2)$, $R=\log(1\mp b)\{\log[(1\mp b)/(1\pm b)]\}^{-1}$, $\beta=½$ and $\alpha=\pi^{-1}\arccos(\pm b/2)$.

Appendix G. MATLAB scripts

MATLAB scripts for the ABR description, abreu_freestream.m and abreu_fit.m, are provided at http://pages.bangor.ac.uk/~oss101/jmSA.html. The abreu_freestream.m script takes the inputs of t ($0\le t<2\pi$) and either (r,φ), (b,φ), or (R,b_1) and returns, the velocity and acceleration, u and a, evaluated at t and also R, b, φ, β and α. All other measures of skewness and asymmetry (u^*_{spike}/U_1^*, a^*_{spike}/A_1^*, S, A_a and A) can be calculated from b and φ (see Table 1). The abreu_fit.m script takes the inputs of R, t ($0\le t<2\pi$) and the velocity, u, that requires fitting to. If t contains more than two elements then a least-squares-fit is be performed. Otherwise fitting is performed on the basis of the position of the maximum, minimum or both. The script, which calls the abreu_freestream.m script, returns the value(s) of b_1 required for the fitting. An example using elfrinknd.m, abreu_fit.m and abreu_fstream.m, abreu_fit_readme.txt, is provided at the above website. MATLAB scripts for the GSSO and GSAW descriptions are also provided.

References

Abreu, T., Silva, P.A., Sancho, F., Temperville, A., 2010. Analytical approximate wave form for asymmetric waves. Coastal Engineering 57 (7), 656–667.

Abreu, T., van der A, D.A., Silva, P.A., Sancho, F., Michallet, H., 2011. New bed shear stress estimator for net sand transport rate predictions under non-linear waves. Journal of Coastal Research SI (64), 2007–2011.

Dalrymple, R.A., 1974. A finite amplitude wave on linear shear current. Journal of Geophysical Research 79 (30), 4498–4504.

Dibajnia, M., Watanabe, A., 1998. Transport rate under irregular sheet flow conditions. Coastal Engineering 35, 167–183.

Dibajnia, M., Moriya, T., Watanabe, A., 2001. A representative wave model for estimation of nearshore local transport rate. Coastal Engineering Journal 43 (1), 1–38.

Doering, J.C., Bowen, A.J., 1995. Parameterization of orbital velocity asymmetries of shoaling and breaking waves using bispectral analysis. Coastal Engineering 26, 15–33.

Drake, T.G., Calantoni, J., 2001. Discrete particle model for sheet flow sediment transport in the nearshore. Journal of Geophysical Research 106 (C9), 19,859–19,868.

Elfrink, B., Hanes, D.M., Ruessink, B.G., 2006. Parameterization and simulation of near bed orbital velocities under irregular waves in shallow water. Coastal Engineering 53, 915–927.

Elgar, S., Guza, R., 1985. Observations of bispectra of shoaling surface gravity waves. Journal of Fluid Mechanics 161, 425–448.

Fuhrman, D.R., Fredsøe, J., Sumer, B.M., 2009. Bed slope effects on turbulent wave boundary layers: 2. Comparison with skewness, asymmetry, and other effects. Journal of Geophysical Research 114, C03025, http://dx.doi.org/10.1029/2008JC005053.

Galan, A., Simarro, G., Orfila, A., 2011. Turbulent bed shear stress under symmetric and asymmetric waves: experimental and numerical results. Journal of Hydraulic Engineering 137 (9), 986–994.

Gonzalez-Rodriguez, D., Madsen, O.S., 2007. Seabed shear stress and bedload transport due to asymmetric and skewed waves. Coastal Engineering 54, 914–929.

Grasmeijer, B.T., Ruessink, B.G., 2003. Modeling of waves and currents in the nearshore parametric vs. probabilistic approach. Coastal Engineering 49, 185–207.

Hoefel, F., Elgar, S., 2003. Wave-induced sediment transport and sandbar migration. Science 299, 1885–1886.

Hsu, T.-J., Hanes, D., 2004. Effects of wave shape on sheet flow sediment transport. Journal of Geophysical Research 109, C05025, http://dx.doi.org/10.1029/2003JC002075.

Isobe, M., Horikawa, K., 1982. Study on water particle velocities of shoaling and breaking waves. Coastal Engineering in Japan 25, 109–123.

Lé Méhauté, B., 1976. An Introduction to Hydrodynamic and Water Waves. Springer, Dusseldorf.

Longuet-Higgins, M.S., Stewart, R.W., 1962. Radiation stress and mass transport in gravity waves, with application to 'surf beats'. Journal of Fluid Mechanics 13, 481–502.

Nielsen, P., 2002. Shear stress and sediment transport calculations for swash zone modelling. Coastal Engineering 45, 53–67.

O'Donoghue, T., Doucette, J.S., van der Werf, J.J., Ribberink, J.S., 2006. The dimensions of sand ripples in full-scale oscillatory flows. Coastal Engineering 53, 997–1012.

Ribberink, J.S., Al-Salem, A.A., 1995. Sheet flow and suspension of sand in oscillatory boundary layers. Coastal Engineering 25 (3–4), 205–225.

Ruessink, B.G., van den Berg, T.J.J., van Rijn, L.C., 2009. Modeling sediment transport beneath skewed asymmetric waves above a plane bed. Journal of Geophysical Research 114, C11021, http://dx.doi.org/10.1029/2009JC005416.

Ruessink, B.G., Ramaekers, G., van Rijn, L.C., 2012. On the parameterization of the free-stream non-linear wave orbital motion in nearshore morphodynamic models. Coastal Engineering 65, 56–63.

Shin, S., Cox, D., 2006. Laboratory observations of inner surf and swash-zone hydrodynamics on a steep slope. Continental Shelf Research 26, 561–573.

Silva, P.A., Abreu, T., van der A, D.A., Sancho, F., Ruessink, B.G., van der Werf, J., Ribberink, J.S., 2011. Sediment transport in nonlinear skewed oscillatory flows: Transkew experiments. Journal of Hydraulic Research 49 (S1), 72–80.

Tajima, Y., Madsen, O.M., 2002. Shoaling, breaking and broken wave characteristics. Proc. 28th ICCE, Cardiff. World Scientific, Singapore, pp. 222–234.

van der A, D.A., O'Donoghue, T., Ribberink, J.S., 2010. Measurements of sheet flow transport in acceleration-skewed oscillatory flow and comparison with practical formulations. Coastal Engineering 57, 331–342.

van der A, D.A., O'Donoghue, T., Davies, A.G., Ribberink, J.S., 2011. Experimental study of the turbulent boundary layer in acceleration-skewed oscillatory flow. Journal of Fluid Mechanics 684, 251–283.

van Rijn, L.C., Tonnon, P.K., Walstra, D.J.R., 2011. Numerical modelling of erosion and accretion of plane sloping beaches at different scales. Coastal Engineering 58, 637–655.